J. Fluid Mech. (1994), *vol.* 280, *pp.* 1–40

Large-eddy simulation of homogeneous turbulence and diffusion in stably stratified shear flow

By H.-J. KALTENBACH, T. GERZ AND U. SCHUMANN
DLR, Institute of Atmospheric Physics, D-82230 Oberpfaffenhofen, Germany

(Received 11 January 1994 and in revised form 30 May 1994)

By means of large-eddy simulation, homogeneous turbulence is simulated for neutrally and stably stratified shear flow at gradient-Richardson numbers between zero and one. We investigate the turbulent transport of three passive species which have uniform gradients in either the vertical, downstream or cross-stream direction. The results are compared with previous measurements in the laboratory and in the stable atmospheric boundary layer, as well as with results from direct numerical simulations. The computed and measured flow properties agree with each other generally within the scatter of the measurements. At strong stratification, the Froude number becomes the relevant flow-controlling parameter. Stable stratification suppresses vertical overturning and mixing when the inverse Froude number based on a turn-over timescale exceeds a critical value of about 3. The turbulent diffusivity tensor is strongly anisotropic and asymmetric. However, only the vertical and the cross-stream diagonal components are of practical importance in shear flows. The vertical diffusion coefficient is much smaller than the cross-stream one at strong stratification. This anisotropy is stronger than predicted by second-order closure models. Turbulence fluxes in downstream and cross-stream directions follow classical mixing-length models.

1. Introduction

Turbulent transport in stably stratified shear flow is anisotropic owing to forcing of downstream turbulent motions by shear and conversion of vertical kinetic energy into potential energy by buoyancy forces (Richardson 1920). As a consequence of stratification, turbulent motions disperse passive species within the flow much quicker in the horizontal directions than in the vertical. The ability of the flow to mix a scalar quantity at different rates depending on the orientation of the gradient of its mean value is commonly considered in terms of the turbulent diffusivity tensor. Quantification of the tensor components in stably stratified shear flow, however, is still an unresolved issue.

Mixing properties of stably stratified shear flows are of interest in many geophysical situations. Stable density stratification, i.e. a situation where lighter fluid lies on top of heavier layers, is predominant in most of the earth's atmosphere and water bodies. Stable stratification tends to suppress turbulent motions. Therefore, mixing will most probably occur in areas with strong shear forcing of turbulence. This situation is often encountered in the upper troposphere and the stratosphere (Lilly, Waco & Adelfang 1974), in the atmospheric boundary layer over cooled surfaces (Ellison 1957), and in the ocean (Monin & Ozmidov 1985).

The knowledge on homogeneous unstratified shear flows has been summarized by Tavoularis & Karnak (1989), based on extensive wind-tunnel studies. For such flows, components of the diffusion tensor have been measured in a wind tunnel by Tavoularis

& Corrsin (1981, 1985) and computed using direct numerical simulation (DNS) by Rogers, Mansour & Reynolds (1989). The tensor components were derived from measuring turbulent heat fluxes caused by superimposing weak temperature gradients to grid-generated turbulence. Webster (1964) was the first to report measurements from stratified shear flows in a heated wind tunnel. However, he could not reach steady-state conditions and the Reynolds number was rather low. Rohr *et al.* (1988*b*) investigated the growth and decay of stably stratified homogeneous shear flows in a salt-stratified water channel. Several experimental studies dealt with unsheared homogeneous decaying turbulence in stratified situations (Stillinger, Helland & Van Atta 1983; Itsweire, Helland & Van Atta 1986; Hopfinger 1987; Lienhard & Van Atta 1990; Yoon & Warhaft 1990). Gerz, Schumann & Elghobashi (1989); Gerz & Schumann (1989, 1991), and Holt, Koseff & Ferziger (1992) numerically simulated homogeneous stably stratified shear flows. They investigated the flow dynamics as a function of Richardson number using DNS.

For neutral shear flows, Corrsin (1974) summarized various theoretical concepts to determine the diffusivity tensor and reviewed older studies. Tavoularis & Corrsin (1985) provided expressions for all components of the diffusivity tensor employing a quasi-Lagrangian analysis. Rubinstein & Barton (1991) applied the renormalization-group theory to determine the diffusivity tensor for shear flows. Models of turbulent diffusion have been deduced using second-order closure (SOC) theory for neutral flows by Galperin (1986), Rogers *et al.* (1989) and Tsarenko & Yaglom (1991), and for stratified turbulence with weak departure from isotropy by Yamada (1977), Freeman (1977), Launder (1978), Tsarenko (1989), and Dörnbrack (1991).

DNS of turbulent flows is restricted to low Reynolds numbers by the need to resolve all scales of motion including the energy dissipation range of the energy spectrum. For example, a grid of 128^3 meshes is required to simulate a flow at a micro-scale Reynolds number $Re_\lambda \leqslant 80$ and Prandtl (or Schmidt) numbers of order 1. Laboratory studies of homogeneous stratified turbulence were conducted for a Reynolds number below about 160 (Rohr *et al.* 1988*b*) or 245 (Tavoularis & Corrsin 1985) at Prandtl numbers of 700 and 0.7, respectively.

A way of studying flows at higher Reynolds numbers which come closer to the ones observed in nature is the method of large-eddy simulation (LES). The three-dimensional time-dependent details of the large eddies, which carry most of the kinetic energy and turbulent fluxes, are computed explicitly in the LES method, whereas a subgrid-scale (SGS) model counts for the effects of small eddies on large eddies. Energy spectra from LES generally develop less steep slopes when approaching the cutoff wavenumber as opposed to DNS spectra. Therefore, given a certain number of degrees of freedom, a LES uses the resources more economically than a DNS where much of the computational effort has to be spent on weakly energetic motions. This becomes particularly important in a stratified flow.

Previous DNS results have been compared with available experimental results on homogeneous turbulence which cover a range of Richardson numbers between 0 and 0.37 (Rohr *et al.* 1988*b*). For higher Richardson numbers, little data for validation of simulation results are available. Holt, Koseff & Ferziger (1992) found a rather strong Reynolds-number dependence of their DNS results. Questions concerning self-similarity or asymptotic behaviour which is a prerequisite for deducing some universal knowledge from the simulation results have not been addressed in detail in the previous work. New concepts, like the transition Richardson number introduced by Holt *et al.* (1992) to separate shear-dominated from buoyancy-dominated flows remain to be tested against a broader database than presently available from DNS.

The main focus of our work is on mixing properties of stably stratified homogeneous turbulence. For this purpose we include passive and active scalars in the domain and solve respective transport equations together with the Navier–Stokes equations. The resulting data allow us to compute the turbulent diffusivity tensor directly which, therefore, can be used to test diffusion models. Besides this, we also intend to augment the knowledge on the dynamics of stratified shear flows in a Richardson-number range between 0 and 1. By using LES we are able to study flows at Reynolds numbers higher than in previous DNS. Some results from accompanying DNS cases will be used to investigate the sensitivity of the LES results to details of the SGS-model.

The method is summarized briefly in §2. The simulation results concerning turbulence dynamics are presented in §3 including a detailed discussion of the role of the Froude number and of the performance of the SGS model. Section 4 treats turbulent diffusion in stably stratified and sheared flow including tests of simple diffusion models. Section 5 finally summarizes the main results from the simulation series.

2. The method and the simulation parameters

Except for the SGS model and the inclusion of three passive species, the method used is as described in Gerz *et al.* (1989), and therefore only the essential features are summarized here. We simulate the turbulent flow in a cubic domain with side lengths L. As indicated in figure 1, the mean velocity $(U(z), 0, 0)$ and the mean temperature $\Theta(z)$ have uniform gradients in the vertical coordinate z while being constant in the two other directions. The three species with mean concentration C_i, $i = 1, 2, 3$, have uniform orthogonal gradients in the Cartesian directions, i.e. $C_i(x_i)$ increases linearly with x_i and is constant in the two other coordinate directions. All gradients of mean species concentrations are kept fixed in time. As explained in Rogers *et al.* (1989), this implies an additional height-dependent source $U(z)\,\mathrm{d}C_1/\mathrm{d}x$ to balance the advection of fluid with smaller concentration from downstream. However, this source does not influence the turbulent fluxes. The turbulent fluctuations relative to these mean values are $u_i = (u, v, w)$ for velocity, θ for temperature and c_i for concentrations. These quantities satisfy periodic boundary conditions at the lateral sides of the computational domain and shear-periodic conditions (i.e. periodicity in a direction which rotates with the mean shear) at the upper and lower boundary. The fluctuations follow the continuity equation for an incompressible fluid with constant density ρ, the equations of motion including buoyancy due to density fluctuations and gravity g in the Boussinesq approximation, and the conservation laws for heat and species concentration as a function of spatial coordinates $x_i = (x, y, z)$ and time t. The density fluctuation is a linear function of temperature with a constant volumetric expansion coefficient β. Coriolis forces as well as molecular diffusion are neglected. From Smagorinsky's closure for modelling of SGS-fluxes we obtain turbulent diffusivities

$$\nu_t = (c_{SGS}\,\Delta)^2 (2 S_{ij}\, S_{ji})^{1/2}, \quad \gamma_{t,\theta} = \gamma_{t,c} = \nu_t / Pr_{SGS}, \tag{1}$$

for velocity, temperature and concentrations, respectively. Here, $S_{ij} = \frac{1}{2}(\partial u_i/\partial x_j + \partial u_j/\partial x_i)$ is the resolved velocity deformation tensor, c_{SGS} is the Smagorinsky coefficient, and Pr_{SGS} is the turbulent Prandtl number of SGS motions. The velocity deformation tensor does not contain the mean shear $\mathrm{d}U/\mathrm{d}z$ (see §3.5 for details of the SGS-model).

The passive scalar c_3 and the temperature θ satisfy identical equations for $\gamma_{t,\theta} = \gamma_{t,c}$. Therefore we get identical statistics when both fields are subject to the same initial

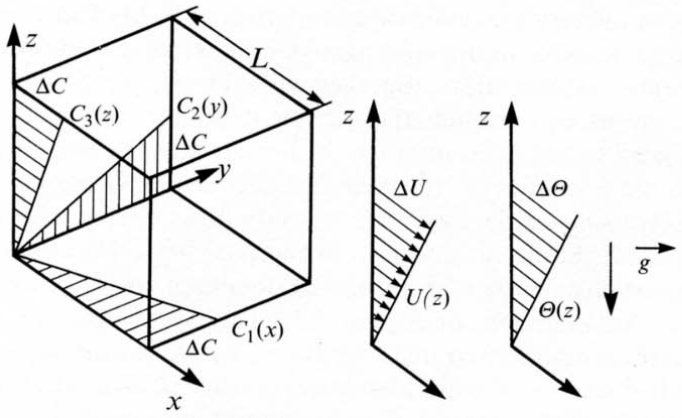

FIGURE 1. Computational domain and mean profiles.

condition. Subsequently, most results are obtained from simulations with only two passive scalars c_1 and c_2 and temperature θ. In §4.3 we address the question of whether a passive scalar c_3 which is initially stochastically independent of the temperature field develops a different transport behaviour to the temperature.

Dimensional quantities refer to L, $\Delta U = LS$, $\Delta\Theta = Ls$, $\Delta C_i = Ls_i$ and S^{-1} as the reference scales for length, velocity, temperature, concentrations and time, respectively, where the constant mean gradients are abbreviated as

$$S = \frac{\mathrm{d}U}{\mathrm{d}z}, \quad s = \frac{\mathrm{d}\Theta}{\mathrm{d}z}, \quad s_1 = \frac{\mathrm{d}C_1}{\mathrm{d}x}, \quad s_2 = \frac{\mathrm{d}C_2}{\mathrm{d}y}. \tag{2}$$

The turbulence is characterized by the effective velocity $q = (\overline{u^2}+\overline{v^2}+\overline{w^2})^{1/2}$ and by the integral lengthscale l,

$$q^2 = 2\int_0^\infty E(k)\,\mathrm{d}k, \quad l = \frac{3}{4}\frac{L}{q^2}\int_0^\infty \frac{E(k)}{k}\,\mathrm{d}k, \tag{3}$$

where $E(k)$ is the energy spectrum as a function of the inverse wavelength or integer spherical wavenumber k.

The initial velocity fields are taken from a simulation of decaying isotropic turbulence at a time when the nonlinear interactions are fully developed. This situation is likely to resemble several laboratory shear-flow configurations (Tavoularis & Karnik 1989; Rohr *et al.* 1988*b*), where the grid-generated turbulence is close to isotropy prior to experiencing shear or buoyancy forces. However, Rogers *et al.* (1989) and Holt *et al.* (1992) showed that about the same results are obtained with initial fields which have not developed nonlinear transfer of energy, as long as the initial shear number is low enough.

Initially isotropic turbulence which instantaneously experiences constant mean shear and density stratification might not be generally representative for all geophysical situations having the same gradient Richardson number. However, it is a well-defined case most likely to show some universal (self-similar) behaviour. The anisotropy of the initial velocity field, e.g. initially purely two-dimensional horizontal motion, enters as an additional parameter which is not a subject of the present study.

Our initial flow field has an energy spectrum $E(k)$ with maximum energy at a wavenumber k corresponding to a wavelength $\frac{1}{9}L$. The turbulence intensity is $q = 0.0261\Delta U$, and the integral lengthscale is $l = 0.0256L$. The corresponding shear

numbers are $Sh = Sl/q = 0.98$ and $Sq^2/\epsilon = 5.04$, where ϵ denotes the dissipation rate of kinetic energy. At wavenumbers up to $k \approx 5$, the energy spectrum increases approximately as $E(k) \sim k^3$. The initial values for the species concentrations and the temperature are set to zero. The effects of using either zero or non-zero initial values for the temperature field and passive scalars are generally small in neutral and stratified shear flows (Gerz & Schumann 1989; Rogers *et al.* 1989; Holt *et al.* 1992).

The equations are integrated numerically using a second-order finite-difference scheme in space and time together with a pseudospectral approximation of the mean advection. The pressure is determined from a Poisson equation such that the continuity equation is satisfied after each timestep, employing a direct Poisson solver. The grid spacing is $\Delta x = L/128$ in all three space directions. The timestep Δt is constant and has a value such that the Courant number $\Delta t\,\Delta U/\Delta x$ equals $\frac{1}{3}$ to $\frac{1}{2}$ (the smaller value for pure shear flow cases because of increasing turbulence velocities). The simulations extend until $St = 12$ requiring 8 hours of computation on a single processor of a Cray Y-MP 2-32.

We present results from five LES with Richardson numbers $Ri = \beta gs/S^2 = 0$, 0.13, 0.25, 0.5 and 1 where the turbulent Prandtl number of the SGS-model is $Pr_{SGS} = 1$. Additionally, two LES ($Ri = 0.13$ and 0.25) are run with $Pr_{SGS} = 0.5$ to test the influence of this model parameter. For reasons discussed in §3.5, the Smagorinsky coefficient is chosen to $c_{SGS} = 0.17$. Further, three DNS with $Ri = 0.13$, 0.25, and 0.5 have been performed (with $Pr = 1$), starting from the same initial fields as the LES. We choose $Re_l = ql/\nu = 89$ for the DNS cases after inspection of the temporal evolution of the mean eddy viscosity and the effective Reynolds number of the LES.

3. Flow dynamics

In this section we present our results concerning basic dynamic properties of the flow and discuss differences between our findings and previously published DNS data (§§3.1 and 3.2). Further, we compare our data with experimental ones in §3.3. Section §3.4 discusses spectral properties of the dynamics and §3.5 considers influences of the SGS model and grid resolution.

3.1. *Results*

We evaluate the simulation data in terms of time series of the ensemble averages approximated by averages over the computational domain of the resolved fields. Ensemble mean values are denoted by bars, root-mean square values by primes, e.g. $u' = \overline{uu}^{1/2}$. Table 1 lists the resultant mean values for three specific times out of the last third of the simulation period of the LES. Temporal mean values and standard deviations of normalized quantities are given in table 2, as obtained by averaging the spatial mean values over the time period $8 \leqslant St \leqslant 12$. Table 3 summarizes key quantities of stratified shear flow as resulting from different simulation methods. The LES results shown are without SGS contributions to avoid ambiguity of their estimates.

Figure 2(*a*, *b*) shows the temporal development of the turbulent kinetic energy, $E_{kin} = \frac{1}{2}q^2$, and of the available potential energy, $E_{pot} = N^2\overline{\theta\theta}/(2s^2)$, as a function of shear time St. For $Ri = 0$, the potential energy is zero by definition in spite of non-zero temperature variance. We find a transition period until $St \approx 3$, during which kinetic energy decreases and potential energy increases strongly. The evolution of the ratio E_{pot}/E_{kin} (figure 2*c*) can be divided in an initial period until $St \approx 5$, which reveals oscillations for the cases with $Ri \geqslant 0.5$, and an 'asymptotic' period for later times when the flows approach constant values depending on Ri. For the pure shear case, the

$Ri =$	0			0.13			0.25			0.5			1		
St	8	10	12	8	10	12	8	10	12	8	10	12	8	10	12
$\overline{u^2}$	4.98	6.32	7.67	2.31	2.35	2.37	1.35	1.24	1.15	0.770	0.609	0.480	0.441	0.318	0.243
$\overline{v^2}$	2.82	3.63	4.71	1.25	1.25	1.30	0.719	0.627	0.546	0.386	0.285	0.213	0.267	0.190	0.145
$\overline{w^2}$	1.60	2.20	3.12	0.610	0.628	0.671	0.356	0.298	0.267	0.194	0.141	0.103	0.135	0.094	0.066
$-\overline{uw}$	1.42	1.84	2.27	0.428	0.448	0.438	0.182	0.162	0.135	0.045	0.021	0.012	−0.005	−0.004	−0.002
$\overline{\theta^2}$	9.98	12.7	16.4	4.72	4.90	5.27	2.53	2.32	2.17	0.946	0.727	0.563	0.304	0.218	0.167
$\overline{c_1^2}$	46.5	65.6	84.2	35.5	44.9	53.1	28.2	32.9	36.7	20.4	22.6	24.3	15.5	17.0	18.2
$\overline{c_2^2}$	18.6	24.2	29.9	14.2	16.4	18.2	11.7	12.7	13.3	9.60	10.1	10.3	9.30	9.98	10.5
$-\overline{w\theta}$	1.83	2.47	3.42	0.519	0.577	0.634	0.176	0.156	0.145	0.020	0.0076	0.0060	−0.0007	−0.0019	−0.0019
$\overline{u\theta}$	4.32	5.42	6.33	1.97	2.05	2.11	1.04	0.998	0.946	0.488	0.389	0.308	0.175	0.127	0.100
$-\overline{uc_1}$	10.9	13.9	16.3	6.46	6.96	7.24	4.16	4.01	3.89	2.48	2.25	2.05	1.68	1.47	1.31
$\overline{wc_1}$	2.22	3.01	4.08	0.426	0.463	0.482	0.144	0.150	0.148	−0.302	−0.257	−0.203	−0.186	−0.132	−0.080
$-\overline{vc_2}$	3.84	4.62	5.78	2.28	2.29	2.38	1.56	1.43	1.31	1.09	0.948	0.822	1.01	0.876	0.770
$-\overline{\theta c_1}$	16.0	21.4	27.4	8.75	9.81	10.8	4.94	4.88	4.84	1.77	1.51	1.27	0.250	0.126	0.064
ϵ	0.911	1.19	1.60	0.387	0.369	0.362	0.235	0.191	0.160	0.132	0.090	0.062	0.078	0.047	0.030
ϵ_θ	3.28	4.39	6.07	1.21	1.19	1.21	0.600	0.497	0.427	0.174	0.117	0.081	0.052	0.031	0.019
ϵ_{c_1}	15.1	23.4	33.3	9.11	11.2	13.0	6.64	7.18	7.46	4.22	4.07	3.83	2.78	2.52	2.28
ϵ_{c_2}	6.05	8.59	11.6	3.76	4.27	4.65	2.97	2.99	2.95	2.17	1.96	1.75	1.80	1.59	1.42
$\overline{\nu}_t$	0.058	0.063	0.070	0.044	0.043	0.043	0.038	0.035	0.033	0.031	0.028	0.024	0.027	0.022	0.019
l	4.57	4.98	5.43	4.04	4.34	4.64	3.66	3.86	3.97	3.28	3.35	3.31	3.22	3.37	3.39
$l_{uu,x}$	6.46	7.04	8.20	4.69	5.09	5.36	4.50	4.92	5.02	4.73	5.02	5.59	5.36	5.98	6.97
Υ	—	—	—	32.9	32.8	33.0	20.0*	18.8*	17.8*	16.9	13.8	11.1	6.3	3.7	2.1

TABLE 1. Spatial mean values obtained from the resolved LES fields at three specific times for $Pr_{SGS} = 1$ (* = 0.5). All quantities refer to the units $10^{-2}L$, $10^{-2}\Delta U$, $L/\Delta U$, $10^{-2}\Delta\Theta$ and $10^{-2}\Delta C$ for length, velocity, time, temperature and species concentration, respectively. Υ in %. The one-dimensional integral lengthscale is computed by $l_{uu,x} = 0.5L\Phi_{uu,x}(k_x = 0)/\overline{uu}$ where $\Phi_{uu,x}$ denotes the variance spectrum of velocity component u in the x-direction.

Ri, (Pr^{SGS})	0, (1)	0.13, (1)	0.13, (0.5)	0.25, (1)	0.25, (0.5)	0.5, (1)	1, (1)
$\overline{u^2}/q^2$	0.517 ± 0.012	0.553 ± 0.003	0.554 ± 0.003	0.570 ± 0.009	0.574 ± 0.009	0.588 ± 0.010	0.529 ± 0.003
$\overline{v^2}/q^2$	0.300 ± 0.003	0.297 ± 0.002	0.298 ± 0.002	0.290 ± 0.005	0.290 ± 0.005	0.275 ± 0.006	0.317 ± 0.001
$\overline{w^2}/q^2$	0.183 ± 0.009	0.149 ± 0.003	0.149 ± 0.002	0.140 ± 0.004	0.136 ± 0.004	0.137 ± 0.004	0.153 ± 0.004
$-\overline{uw}/q^2$	0.151 ± 0.002	0.105 ± 0.002	0.106 ± 0.002	0.075 ± 0.002	0.074 ± 0.003	0.022 ± 0.006	-0.005 ± 0.001
$-\overline{uw}/u'w'$	0.493 ± 0.011	0.365 ± 0.007	0.369 ± 0.007	0.264 ± 0.006	0.266 ± 0.008	0.076 ± 0.020	-0.019 ± 0.004
$-\overline{w\theta}/w'\theta'$	0.467 ± 0.006	0.323 ± 0.010	0.369 ± 0.009	0.187 ± 0.004	0.244 ± 0.004	0.031 ± 0.008	-0.013 ± 0.007
$\overline{u\theta}/u'\theta'$	0.600 ± 0.015	0.603 ± 0.005	0.635 ± 0.005	0.585 ± 0.012	0.620 ± 0.010	0.584 ± 0.007	0.484 ± 0.006
$-\overline{uc}_1/u'c_1'$	0.682 ± 0.022	0.679 ± 0.022	0.718 ± 0.021	0.636 ± 0.023	0.674 ± 0.023	0.609 ± 0.008	0.631 ± 0.006
$\overline{wc}_1/w'c_1'$	0.252 ± 0.002	0.086 ± 0.003	0.106 ± 0.003	-0.048 ± 0.002	-0.032 ± 0.002	-0.141 ± 0.007	-0.102 ± 0.018
$-\overline{vc}_2/v'c_2'$	0.501 ± 0.015	0.510 ± 0.018	0.551 ± 0.018	0.511 ± 0.014	0.553 ± 0.016	0.561 ± 0.004	0.634 ± 0.006
$-\overline{\theta c}_1/\theta'c_1'$	0.740 ± 0.002	0.662 ± 0.001	0.677 ± 0.011	0.563 ± 0.013	0.574 ± 0.016	0.372 ± 0.019	0.069 ± 0.026
D_{11}/D_{22}	2.93 ± 0.067	3.00 ± 0.080	3.01 ± 0.087	2.80 ± 0.078	2.86 ± 0.097	2.38 ± 0.069	1.68 ± 0.014
D_{33}/D_{22}	0.531 ± 0.034	0.247 ± 0.011	0.269 ± 0.012	0.110 ± 0.004	0.136 ± 0.004	0.011 ± 0.004	-0.002 ± 0.001
$-D_{13}/D_{22}$	1.15 ± 0.024	0.887 ± 0.014	0.892 ± 0.016	0.695 ± 0.015	0.709 ± 0.016	0.411 ± 0.024	0.148 ± 0.014
D_{31}/D_{22}	-0.646 ± 0.040	-0.198 ± 0.007	-0.229 ± 0.010	0.104 ± 0.009	0.070 ± 0.006	0.266 ± 0.009	0.146 ± 0.025
$2E_{pot}/\overline{w^2}$	0	1.01 ± 0.018	0.834 ± 0.020	1.91 ± 0.084	1.62 ± 0.084	2.57 ± 0.087	2.39 ± 0.086
B/χ	—	0.952 ± 0.059	1.03 ± 0.053	—	0.782 ± 0.024	0.147 ± 0.033	-0.110 ± 0.061
Ri_f	0	0.167 ± 0.009	0.171 ± 0.009	0.243 ± 0.003	0.284 ± 0.010	0.222 ± 0.023	—
Pr_t	0.741 ± 0.033	0.781 ± 0.041	0.764 ± 0.037	1.03 ± 0.014	0.882 ± 0.028	2.28 ± 0.25	—
F	1.54 ± 0.048	0.999 ± 0.031	1.00 ± 0.033	0.694 ± 0.021	0.695 ± 0.020	0.232 ± 0.036	-0.073 ± 0.013
c_N	—	0.325 ± 0.012	0.337 ± 0.011	0.258 ± 0.005	0.310 ± 0.007	0.049 ± 0.013	-0.019 ± 0.011
c_h	—	0.200 ± 0.016	0.207 ± 0.016	0.203 ± 0.008	0.246 ± 0.013	0.054 ± 0.012	-0.039 ± 0.021
A_S	0.540 ± 0.016	0.587 ± 0.027	0.589 ± 0.029	0.638 ± 0.015	0.631 ± 0.022	0.635 ± 0.025	0.508 ± 0.045

TABLE 2. Spatial and temporal mean values and standard deviations of normalized quantities from LES cases. The time-averaging interval is $8 < St < 12$.

Quantity	Simulation/Ri	0	0.13 (0.11)	0.25	0.5	1
F	LES 128^3	1.54 ± 0.05	1.00 ± 0.03	0.63 ± 0.02	0.19 ± 0.04	-0.03 ± 0.01
	DNS 128^3	—	0.99 ± 0.04	0.53 ± 0.03	-0.03 ± 0.08	—
	Holt *et al.* (1992)	1.8 ± 0.1	0.9	0.3 ± 0.15	0 ± 0.2	-0.2 ± 0.1
	LES 96^3	1.70 ± 0.02	0.93 ± 0.05	0.57 ± 0.03	0.18 ± 0.04	0.01 ± 0.04
	DNS 96^3	1.57 ± 0.08	0.80 ± 0.04	0.39 ± 0.03	-0.01 ± 0.08	-0.14 ± 0.05
$-\overline{w\theta}/w'\theta'$	LES 128^3	0.47 ± 0.01	0.32 ± 0.01	0.19 ± 0.00	0.03 ± 0.01	-0.01 ± 0.01
	DNS 128^3	—	0.33 ± 0.01	0.18 ± 0.01	-0.04 ± 0.02	—
	Holt *et al.* (1992)	0.5	0.32	0.09	-0.08	-0.05
	LES 96^3	0.48 ± 0.00	0.30 ± 0.01	0.16 ± 0.01	0.03 ± 0.00	-0.005 ± 0.017
	DNS 96^3	0.47 ± 0.01	0.31 ± 0.01	0.17 ± 0.00	-0.02 ± 0.01	-0.03 ± 0.03
$-\overline{uw}/u'w'$	LES 128^3	0.49 ± 0.01	0.37 ± 0.01	0.26 ± 0.00	0.08 ± 0.02	-0.02 ± 0.00
	DNS 128^3	—	0.37 ± 0.01	0.24 ± 0.02	-0.03 ± 0.04	—
	Holt *et al.* (1992)	0.55	0.38	0.16 ± 0.04	-0.16	-0.08
	LES 96^3	0.50 ± 0.00	0.33 ± 0.00	0.23 ± 0.01	0.07 ± 0.01	-0.003 ± 0.010
	DNS 96^3	0.49 ± 0.01	0.32 ± 0.00	0.20 ± 0.01	-0.01 ± 0.03	-0.07 ± 0.01
$\overline{uu}/\overline{ww}$	LES128^3	2.8 ± 0.2	3.7 ± 0.1	4.1 ± 0.2	4.3 ± 0.2	3.5 ± 0.1
	DNS 128^3	—	4.3 ± 0.1	5.4 ± 0.5	6.2 ± 0.5	—
	Holt *et al.* (1992)	3.6	6 ± 0.5	9.5 ± 1	6.8 ± 0.1	3.6 ± 0.2
	LES 96^3	3.9 ± 0.2	4.8 ± 0.1	4.9 ± 0.2	4.7 ± 0.2	3.5 ± 0.1
	DNS 96^3	3.7 ± 0.2	5.4 ± 0.0	6.1 ± 0.5	6.2 ± 0.5	4.3 ± 0.3
$2E_{pot}/\overline{ww}$	LES 128^3	0	1.0 ± 0.0	1.9 ± 0.1	2.6 ± 0.1	2.4 ± 0.1
	DNS 128^3	—	1.1 ± 0.0	2.2 ± 0.2	3.1 ± 0.2	—
	Holt *et al.* (1992)	0	1.5	4.0 ± 0.5	3.8 ± 0.2	2.8 ± 0.2
	LES 96^3	0	1.3 ± 0.0	2.3 ± 0.1	2.7 ± 0.1	2.4 ± 0.1
	DNS 96^3	0	1.4 ± 0.0	2.6 ± 0.2	3.2 ± 0.1	2.5 ± 0.2

TABLE 3. Comparison of key quantities obtained from different simulations. Temporal mean values from the interval $8 < St < 12$ (Holt *et al.*'s (1992) data from $10 < St < 14$). $Re_l = ql/\nu = 89, 57, 70$, for DNS 128^3, Holt *et al.* (1992), DNS 96^3, respectively; $Pr = Pr_{SGS} = 1$.

kinetic energy increases exponentially. At $Ri = Ri_S \approx 0.13$, the 'stationary' Richardson number, E_{kin} and, to a lesser degree, also E_{pot} become approximately constant. We will refer to cases with $Ri > (<) Ri_S$ as supercritical (subcritical). E_{kin} and E_{pot} decrease for $Ri > 0.13$. Comparing LES with DNS results it is found that both methods show almost identical energy levels for $Ri = 0.13$, but that the energies decay at stronger rates in the DNS compared to the LES when Ri is supercritical.

The energy distribution among the variances $\overline{uu}$, $\overline{vv}$ and $\overline{ww}$ reaches almost constant ratios $\overline{u_i^2}/q^2$ (table 2). The anisotropy expressed in terms of $K_{ij} = \overline{u_i u_j}/q^2$, increases slightly up to $Ri = 0.5$. Our corresponding DNS reaches similar anisotropy levels as the LES for $Ri = 0.13$ (table 3). However, for higher Ri, the vertical velocity is much more damped in the DNS than in the LES.

The growth rate parameter

$$F = \frac{P-B}{\epsilon}, \quad \text{where} \quad P = -\overline{uw}S, \quad B = -\beta g \overline{w\theta}, \tag{4}$$

controls the rate of change of kinetic energy (equation (29) in the appendix). $F = 1$ implies constant kinetic energy. The growth rate becomes approximately stationary for $St > 6$. F is less than unity for $Ri > Ri_S$, and about $F = 1.5\pm0.05$ for neutral shear flow

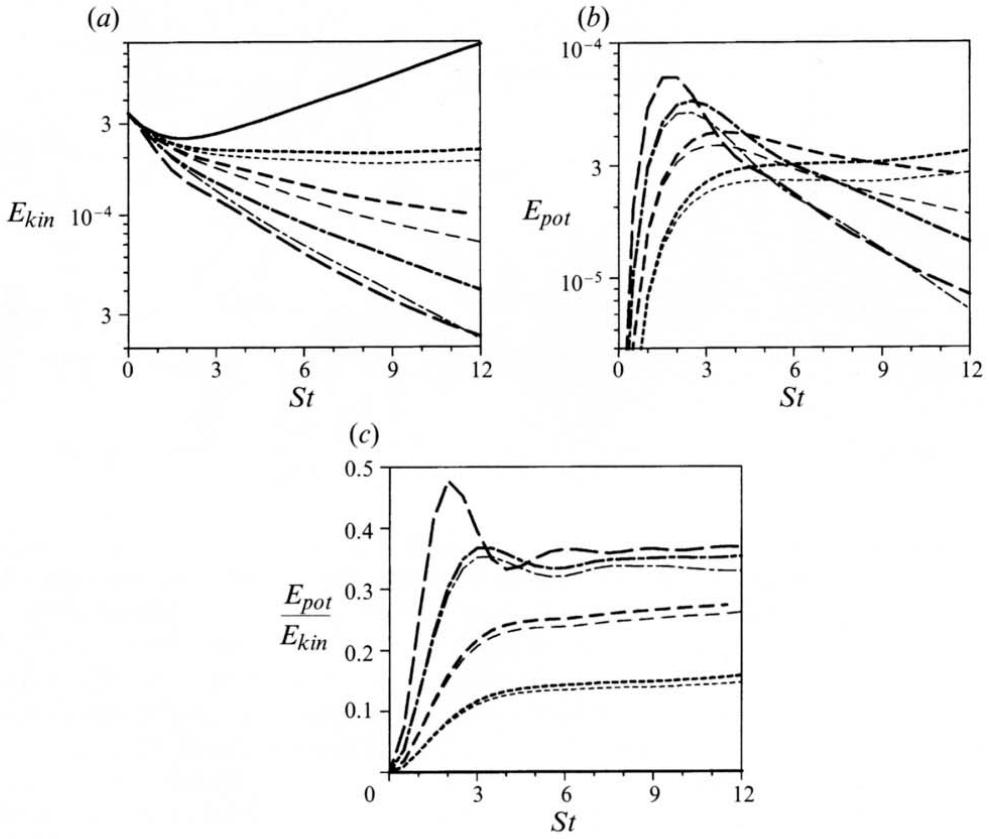

FIGURE 2. (*a*) Kinetic energy, (*b*) potential energy and (*c*) ratio of potential and kinetic energy versus time in shear-rate units, St, for various Richardson numbers: ——, $Ri = 0$ (LES); ---, 0.13 (LES and DNS); – – –, 0.25 (LES and DNS); — · —, 0.5 (LES and DNS); — — —, 1 (LES). Thick lines: LES results; thin lines: DNS results.

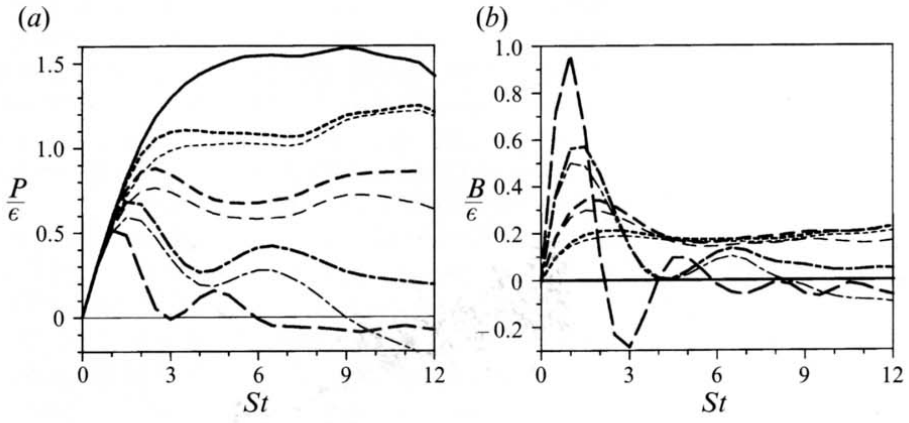

FIGURE 3. (*a*) Shear production P/ϵ and (*b*) buoyancy term B/ϵ, normalized by the dissipation rate, versus St. Line coding as in figure 2.

(table 2). In figure 3 we show the evolution of the ratios P/ϵ and B/ϵ versus St. This plot gives detailed information on the relative importance of the three terms P, B, and ϵ in the energy budget. In moderately stratified flows with $Ri \leqslant 0.25$, the production term P has roughly the same magnitude as the energy sink ϵ, whereas the buoyancy

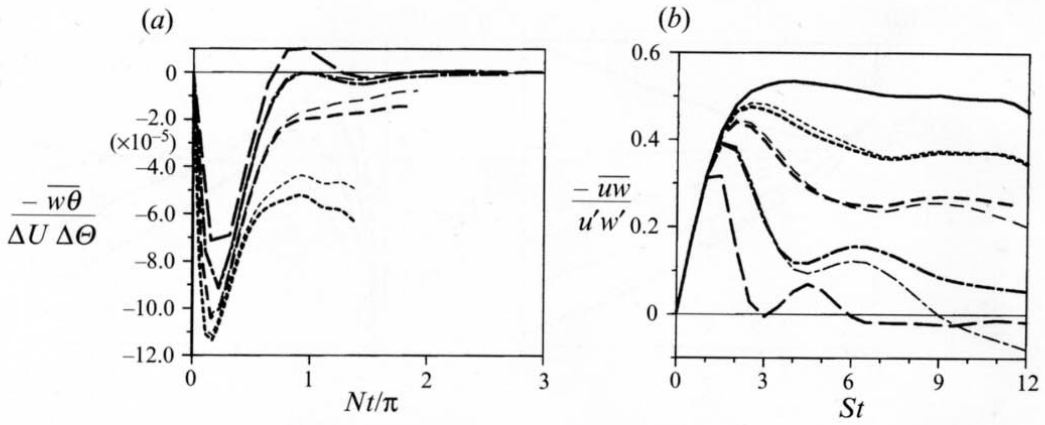

FIGURE 4. (*a*) Vertical heat flux $-\overline{w\theta}/(\Delta U\,\Delta\Theta)$ versus Nt/π. (*b*) Correlation coefficient $-\overline{uw}/(u'w')$ versus St. Line coding as in figure 2.

term B never exceeds 20% of ϵ in the asymptotic flow region ($St > 6$). For cases with $Ri > 0.5$, P and B are smaller than ϵ except during the first buoyancy period when B plays an important role in the energy budget. The ratio of buoyancy production B and dissipation rate of potential energy $\chi = \frac{1}{2}(N^2/s^2)\,\epsilon_\theta$, B/χ, decreases from 1 at $Ri = 0.13$ to less than 0.15 at $Ri = 1$ (table 2). The late stages of the LES with $Ri = 1$ and the DNS with $Ri = 0.5$ are dominated by the dissipative terms because the absolute values of P/ϵ, B/ϵ, and B/χ do not exceed 15%. The maximum value of $Ri_f = B/P$ is close to 30% in our simulations. This corroborates the important findings by Rohr (1985) and Holt *et al.* (1992) that the buoyancy term B plays a minor role in the kinetic-energy budget of stratified shear flows and that the main impact of buoyancy on the development of the kinetic energy is rather indirect through reduction of the production term P.

Time series of shear stress $\overline{uw}$ and vertical heat flux $\overline{w\theta}$ reveal the strong influence of buoyancy on these quantities. The evolution of $\overline{w\theta}$, as plotted in figure 4(*a*) versus time scaled by half the buoyancy period, π/N, emphasizes the rapid decrease of the flux magnitude for increasing Ri. In all cases, vertical fluxes reach maximum magnitudes at approximately $Nt/\pi = 0.25$. Figure 4(*b*) shows the evolution of the correlation coefficient of $-\overline{uw}$. All data collapse on one curve for $0 < St < 1$. Figures 3 and 4 reveal that in both LES and DNS vertical turbulent fluxes may change their sign and become persistently positive, i.e. counter-gradient. We find only slight differences in the evolution of correlation coefficients of LES and DNS cases with $Ri \leqslant 0.25$. However, fluxes become counter-gradient for $Ri = 0.5$ in the DNS whereas they stay weakly down-gradient in the LES at this Richardson number.

When comparing the magnitudes of counter-gradient fluxes with the most negative values of the fluxes, which were reached at times around $Nt/\pi \approx 0.24$ (see figure 4*a*), we find that the persistent positive fluxes amount to less than 1% of the strong down-gradient fluxes that occurred in the early flow period. This holds for both LES and DNS. This small ratio has certainly to be taken into account when discussing the relevance of counter-gradient fluxes.

Figure 5(*a*) depicts ratios of turbulent diffusivities and molecular or SGS-eddy diffusivities versus Ri at $St = 11$ for DNS and LES. The ratios do not change much for $St > 6$. It turns out that turbulent vertical fluxes of heat and momentum become smaller than their molecular counterparts in the DNS with $Ri \geqslant 0.25$. Flux ratios of LES cases are approximately twice as high as in the DNS. Resolved scale fluxes are still

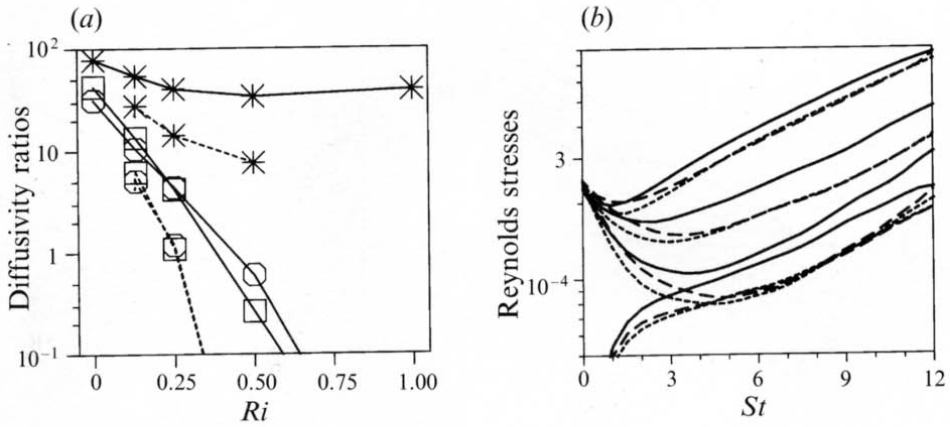

FIGURE 5. (*a*) Ratios of resolved turbulent and SGS-eddy diffusivities (LES data, solid lines) and of turbulent and molecular diffusivities (DNS data, dashed lines) versus Ri at $St = 11$; ○, momentum (K_m/ν); □, heat (K_h/γ); ✱, spanwise diffusivity (D_{22}/γ_c). (*b*) Reynolds stresses $\overline{u^2}$, $\overline{v^2}$, $\overline{w^2}$, $-\overline{uw}$ (from top to bottom) versus St for $Ri = 0$; ——, LES with 128^3 meshes; ---, LES with 96^3 meshes; –––, DNS with 96^3 meshes.

a factor of five higher than SGS-fluxes for $Ri = 0.25$. However, vertical (resolved) turbulent fluxes become smaller than SGS-contributions for $Ri \geqslant 0.5$. Therefore, at late times the sum of the fluxes at resolved scales and at subgrid or molecular scales always remain down-gradient in both DNS and LES for all Ri under consideration.

3.2. *Discussion*

The dynamics of stably stratified and sheared turbulence have been discussed for laboratory experiments in Rohr *et al.* (1988*b*) and for DNS results in Gerz *et al.* (1989), Gerz & Schumann (1991), and Holt *et al.* (1992). The dynamics can be understood in terms of the transport equations for variances and covariances, which are given in the Appendix.

3.2.1. *LES versus DNS*

The dynamical results are similar to what has been described before on the basis of DNS. However, with increasing strength of stratification, differences between LES and DNS become more pronounced. As listed in table 3, the DNS data reported by Holt *et al.* (1992) show 60 % higher anisotropy levels, expressed as the ratio $\overline{uu}/\overline{ww}$, than our LES data for Ri in between 0.13 and 0.5. They develop a 17 % higher growth rate parameter F in the neutral case but considerably smaller values than our LES for $Ri \geqslant 0.25$. The correlation coefficients of vertical fluxes of momentum and heat are 30–50 % smaller in Holt *et al.*'s DNS for $Ri = 0.25$ compared to our LES. Further, our fine grid DNS data also differ significantly from Holt *et al.*'s DNS results although both simulations provided the same numerical resolution of 128^3 meshes. However, they come closer to the values obtained from our coarse grid DNS results with 96^3 meshes. From the work by Shirani, Ferziger & Reynolds (1981) and Rogers, Moin & Reynolds (1986) it is known that the development of neutral homogeneous shear flow is quite sensitive to dissipative processes which occur in the initial stage of flow development. In figure 5(*b*) the evolution of the variances $\overline{u_i^2}$ is plotted for neutrally stratified shear flows simulated with different grid resolution and Reynolds numbers. The figure gives some hints as to how a strong initial dissipation rate influences growth rates. Generally, the variances drop to lower values in the low Re cases before they start

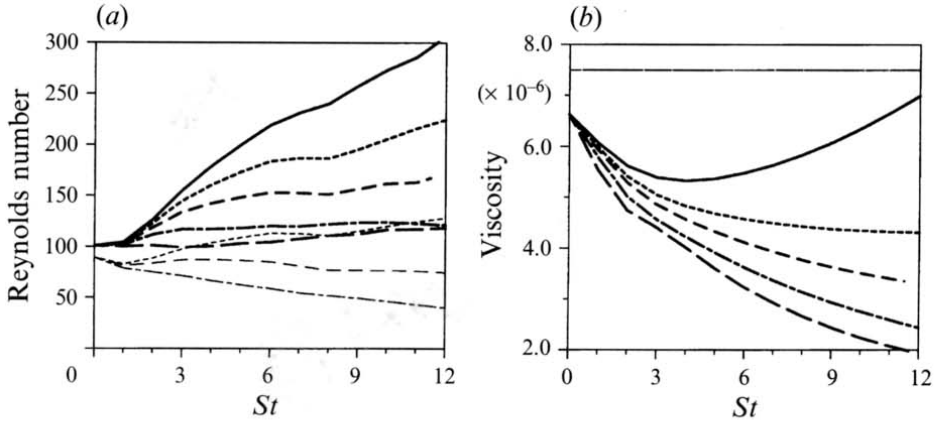

FIGURE 6. (*a*) Effective Reynolds number $ql/\overline{\nu_t}$ (LES) and Reynolds number ql/ν (DNS) versus St; (*b*) mean turbulent viscosity $\overline{\nu_t}/(\Delta UL)$ (LES) and molecular viscosity $\nu/(\Delta UL)$ (DNS) versus St. Line coding as in figure 2.

growing. This drop is more pronounced for $\overline{ww}$ than for $\overline{uu}$ leading to higher anisotropy levels K_{ij} in the coarse grid simulations. Hence, the differences between our DNS results and Holt *et al.*'s (1992) data are most probably due to Reynolds number differences. In fact, the initial Reynolds number of our 128^3 DNS, based on q and l is 89 compared to 57 in Holt *et al.*'s simulations. Re_l was around 70 in our 96^3 DNS. Holt *et al.* (1992) also performed simulations with higher Reynolds numbers, which agree better with our data, but most of their results are reported for the rather low Reynolds-number case.

Our DNS and LES results agree well for $Ri = 0.13$ (and smaller subcritical values, see Kaltenbach 1992) but diverge for supercritical Richardson numbers. This can be understood by examining the behaviour of the mean turbulent viscosity $\overline{\nu_t}$ and related Reynolds numbers, see figure 6. Although our LES is nominally free of viscous forces because the molecular fluxes are neglected, there exists an effective Reynolds number for the resolved turbulent motions, $Re = ql/\overline{\nu_t}$, which increases with time from 100 to about 300 for neutral flow but stays about constant at $Ri = 1$. The Reynolds number based on the molecular viscosity ν obtained from DNS increases slowly for $Ri = 0.13$, but decreases in time when Ri is supercritical. The effective Re of the LES generally evolves to larger values than Re of the DNS which is mainly due to the temporal behaviour of the turbulent viscosity (figure 6*b*). In the most stable case, $\overline{\nu_t}$ reduces by 60% of its initial value during the flow evolution, whereas it resumes its initial value at late times for $Ri = 0$. Therefore, more significant deviations between LES and DNS are expected in the more stable cases.

Turbulent flows exposed to mean shear and stratification are temporally evolving and, hence, do not reach stationary states (except for Ri_S). Nevertheless, quasi-stationary states can often be achieved when normalized quantities such as correlation coefficients, anisotropy measures like K_{ij} or ratios such as F, P/ϵ and B/ϵ reach stationary values. Our simulated flows achieve quasi-steady states after $St = 6$ for $0 \leqslant Ri \leqslant 0.25$. This indicates that the flow is in an asymptotic state where the properties are fixed by the value of Ri. Deviations from quasi-stationarity are observed for $Ri \geqslant 0.5$. However, compared to the present DNS data and those of Gerz *et al.* (1989), Gerz & Schumann (1991) and Holt *et al.* (1992), the LES results fulfil the criterion of quasi-stationarity better. This effect is due to the SGS-model which reduces dissipation when the turbulence activity decreases.

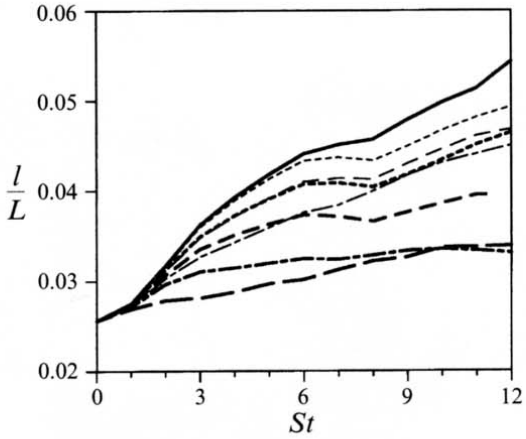

FIGURE 7. Integral lengthscale l/L versus St with line coding as in figure 2.

Turbulent eddies change their shape under the influence of mean shear towards inclined vortex tubes. This leads to an increasing integral lengthscale l. Figure 7 shows how stable stratification reduces the growth rate of l. The fact that l grows at about constant rate during the period $3 < St < 12$ in the neutral case (where the growth rate is largest) indicates that the computational domain is large enough to cover all relevant large-scale motion components.

The collapse of shear stress and vertical heat flux for $Ri \geqslant 0.5$ demonstrates the decrease of vertical mixing, i.e. the ability of the flow to move heavier (colder) fluid over lighter (warmer) fluid. Holt *et al.* (1992) introduced the volume fraction Υ of convectively overturning turbulence, i.e. statically unstable regions, where $\partial(\Theta+\theta)/\partial z$ is negative. Whereas the fluid is convectively mixed at more than 35% of the gridpoints in the neutral case, Υ amounts to less than 5% for $Ri = 1$ at late times (see table 1). The extinction of vertical overturning motion for large static stability is illustrated by iso-surface plots of the total temperature $\Theta(z)+\theta$ in figure 8. Little sign of convective zones is found in the $Ri = 1$ case. The surface pattern indicates wavy motions with a larger wavelength in the downstream than in the cross-stream direction.

3.2.2. *Multiple time-scale problem*

Holt *et al.* (1992) noted that the stratified shear flow is a multiple timescale problem. The outer timescales are S^{-1} and N^{-1}, where $N = (\beta g\, \mathrm{d}\Theta/\mathrm{d}z)^{1/2}$ is the Brunt–Väisälä frequency. The internal timescale of turbulence may be either a turnover scale, $\tau = l/q$, or a dissipative scale, $\tau_\epsilon = q^2/(2\epsilon)$. The internal and outer scales are related by the shear number Sh and the inverse Froude number Fi,

$$Sh = S\tau, \quad Fi = Fr^{-1} = N\tau, \quad Ri = \frac{N^2}{S^2} = \frac{Fi^2}{Sh^2}. \tag{5}$$

Here, the gradient-Richardson number Ri measures the ratio of the outer timescales. In the present simulations, the flow state varies at constant Richardson number with increasing internal timescale τ. Cases with different values of Ri reach the same value of Fi or Sh at different times St. None of the three numbers Ri, Sh and Fi, which are related through (5), can be changed independently of each other. Gerz *et al.* (1989) and Holt *et al.* (1992) identified Ri as the primary dimensionless parameter in stratified shear flow. Ivey & Imberger (1991) found that the Froude number, which is the

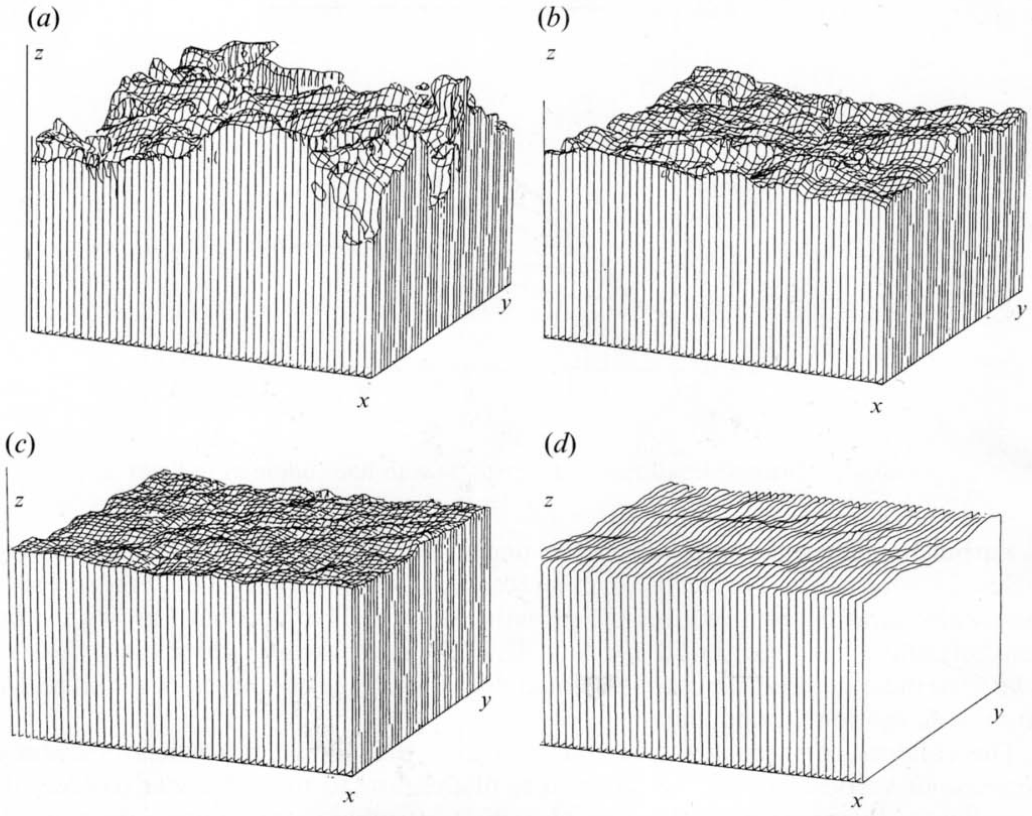

FIGURE 8. Perspective views of iso-surfaces of temperature $\theta+\Theta = 0.25\Delta\Theta$ in a subdomain with side-lengths $\frac{1}{2}L$ at $St = 12$ for various Richardson numbers. These results are from simulations with 96^3 grid points. (*a*) $Ri = 0$, (*b*) $Ri = 0.25$, (*c*) $Ri = 0.5$, (*d*) $Ri = 1$.

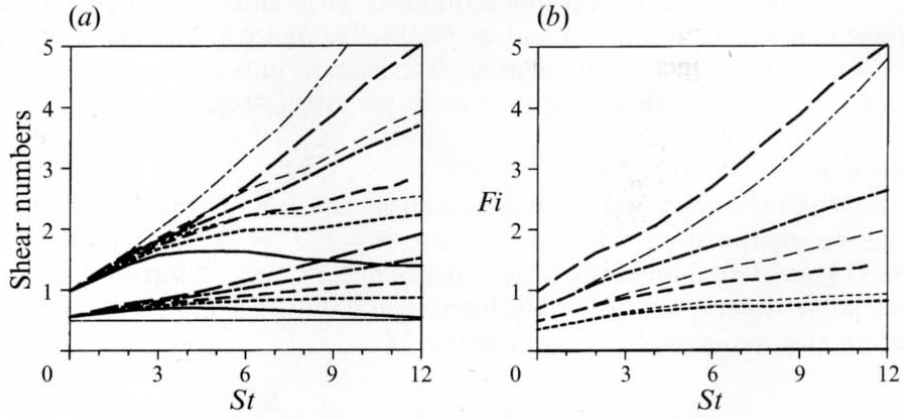

FIGURE 9. (*a*) Shear number $Sh = Sl/q$ (upper curves) and SGS shear-number $Sh_{SGS} = S\Delta x/(2e)^{0.5}$ (lower curves) versus St, (*b*) inverse Foude number $Fi = Nl/q$ versus St. Line coding as in figure 2.

relevant parameter for shear-free stratified turbulence (Hopfinger 1987; Yoon & Warhaft 1990), is also well-suited for the characterization of stratified flows with considerable mean shear. Our results corroborate these findings.

The turnover timescale τ increases with time if $Ri > Ri_S$, because the integral-length scale l grows monotonically for all Ri and q decreases for $Ri > Ri_S$. Figure 9 shows how the change in timescale affects the evolution of Sh and Fi. Both become nearly constant

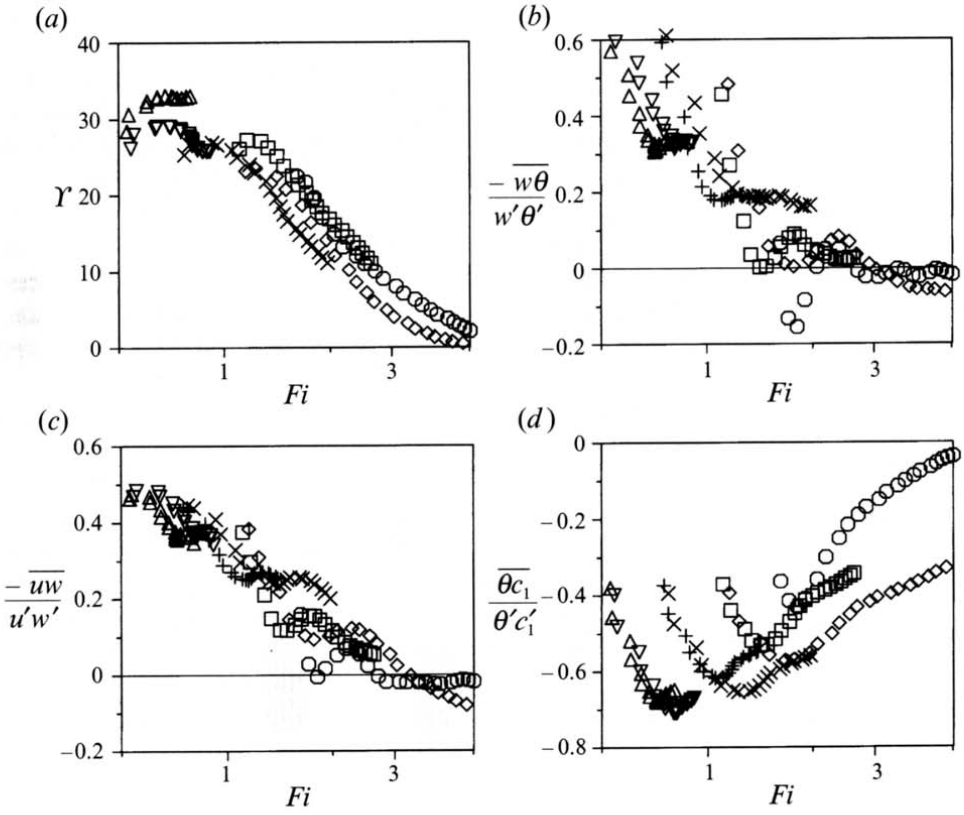

FIGURE 10. Percentage of convective instabilities $\Upsilon(a)$, correlation coefficients of vertical fluxes of heat (b), downstream momentum (c), and correlation coefficient $\overline{\theta c_1}/(\theta' c_1')$ (d) versus inverse Froude number Fi at $St \geqslant 2$. Symbols for LES: △, $Ri = 0.13$; +, 0.25; □, 0.5; ○, and 1; symbols for DNS; ▽, $Ri = 0.13$; ×, 0.25; ◇, 0.5. All data for $Pr_{SGS} = 1$.

for $Ri = 0$ and 0.13 and increase otherwise. The higher decay rate of q in the DNS causes τ to grow faster for $Ri = 0.5$ compared to the LES.

The fact that Fi grows when Ri is supercritical indicates that a true asymptotic state might not be expected for supercritical cases because the timescale ratio continuously changes in every decaying flow. Indeed, in the LESs with $Ri \geqslant 0.5$ we find slight trends in the time series of P/ϵ, B/ϵ, $-\overline{uw}/(u'w')$, and F (even if the buoyancy-induced oscillations are filtered out). Each of the simulations is characterized by a distinct evolution of Fi with time. Therefore Fi can be chosen instead of time as the independent variable to characterize the evolution of a stratified flow.

Figure 10 shows how the volume fraction Υ, the correlation coefficients for heat and momentum fluxes and the correlation coefficients for the cross correlation $\overline{\theta c_1}$ evolve as functions of Fi. Flows with almost constant Fi, like the $Ri = 0.13$ case, settle near a single point in this type of diagram, whereas decaying stratified cases approach the highest values of Fi at $St = 12$. In contrast to the plots versus St or Nt/π, the curves have no common start point owing to the different initial values of Fi. It is noteworthy that the results for different Ri cases line up in one single band when plotted versus Fi. Ivey & Imberger (1991) obtained similar results when plotting the flux-Richardson number or the heat-flux correlation coefficient versus the turbulent Froude number. Figure 10 also shows that both the momentum flux and the heat flux decay quickly for $Fi > 1$ and become practically zero or counter-gradient for a critical inverse Froude

number Fi_{crit} in between 2 and 3, independent of time, Richardson number or simulation method.

Figure 9(*b*) together with figure 10(*b*, *c*) shows that the LES always provide smaller values of Fi (i.e. show stronger mixing at a given time) than the corresponding DNS. The differences in Fi are particularly large at supercritical Richardson numbers for $St \geqslant 6$. They are the reason why DNS and LES with the same value of Ri reach different heat-flux and momentum-flux correlation coefficients (i.e. mixing properties) at a given time. However, we believe that the LESs would eventually follow the same evolution path as the DNS when time exceeds $St = 12$. Similar conclusions can be drawn from studying the flow evolution in terms of Froude number versus Reynolds number or in hydrodynamic phase diagrams as in Ivey & Imberger (1991) and Itsweire *et al.* (1993).

In summary, we conclude that the Froude number becomes at least as important as the Richardson number when the stratification becomes strong. We do not think that the definition of a 'transition' Richardson number as proposed by Holt *et al.* (1992) helps much for interpretation of shear flow data. The fact that Ri_{trans} depends on the Reynolds number can be interpreted in terms of Froude-number differences between low- and high-Reynolds-number cases. For the purpose of determining 'characteristic' flow properties at a certain value of Ri it is important to have rather slowly varying Froude numbers. This is the case in our LES with Ri in between 0.13 and 0.25. Conversely, one has to be cautious when analysing DNS data at low Reynolds number (as Holt *et al.*'s (1992) DNS with $Ri = 0.25$) since these flows are in transient states.

3.2.3. *Asymptotic flow stages*

In the previous section we discussed the influence of the Froude number on asymptotic or self-similar flow stages. Here we want to widen the discussion and consider the influence of flow history. We ask whether the ratio of potential and kinetic energy reaches a characteristic 'asymptotic' value that is uniquely determined by the Richardson or Froude number. As was pointed out before, the magnitude of turbulent fluxes may change drastically during flow evolution. In cases with $Ri \geqslant 0.5$, the flux terms P and B mainly contribute to the balances of kinetic and potential energy in the early flow period, $0 < St < 5$ (figure 3), which will therefore subsequently be referred to as 'mixing-dominated'. Later, in the 'decay-dominated' flow regime, dissipative processes dominate the evolution of kinetic and potential energy. The ratio E_{pot}/E_{kin} reaches its 'asymptotic' value at $St \approx 5$, i.e. during the mixing-dominated period. The ratio does not change much in the decay-dominated period because the ratio of dissipation rates, χ/ϵ, closely matches the ratio of energies, E_{pot}/E_{kin}, and because flux terms are small for $St > 5$. Hence, the energy ratio at late times is controlled by the mixing-dominated flow state and, therefore, depends on the flow history and does not necessarily reflect a 'natural' balance between potential and kinetic energy.

Holt *et al.* (1992) did not find any significant change in the 'asymptotic' value of $\eta = 2E_{pot}/\overline{ww}$ when they changed the initial ratio of potential to kinetic energy drastically. This would indicate that the asymptotic value of η is indeed quite universal for a given Richardson number. On the other hand, Holt's data (Holt 1990) also reveal that the evolution of $\overline{uw}/u'w'$ does not depend on the initial value of η at all. Hence, the early flow is controlled by the interaction of the initially isotropic velocity field with the mean shear. It is likely, therefore, that other initial fields (e.g. purely two-dimensional) may result in other asymptotic flow stages.

The importance of the initial phase for the structure at late times is illustrated further by figure 11. It shows the field of the species concentration fluctuation c_1 at $St = 12$ for

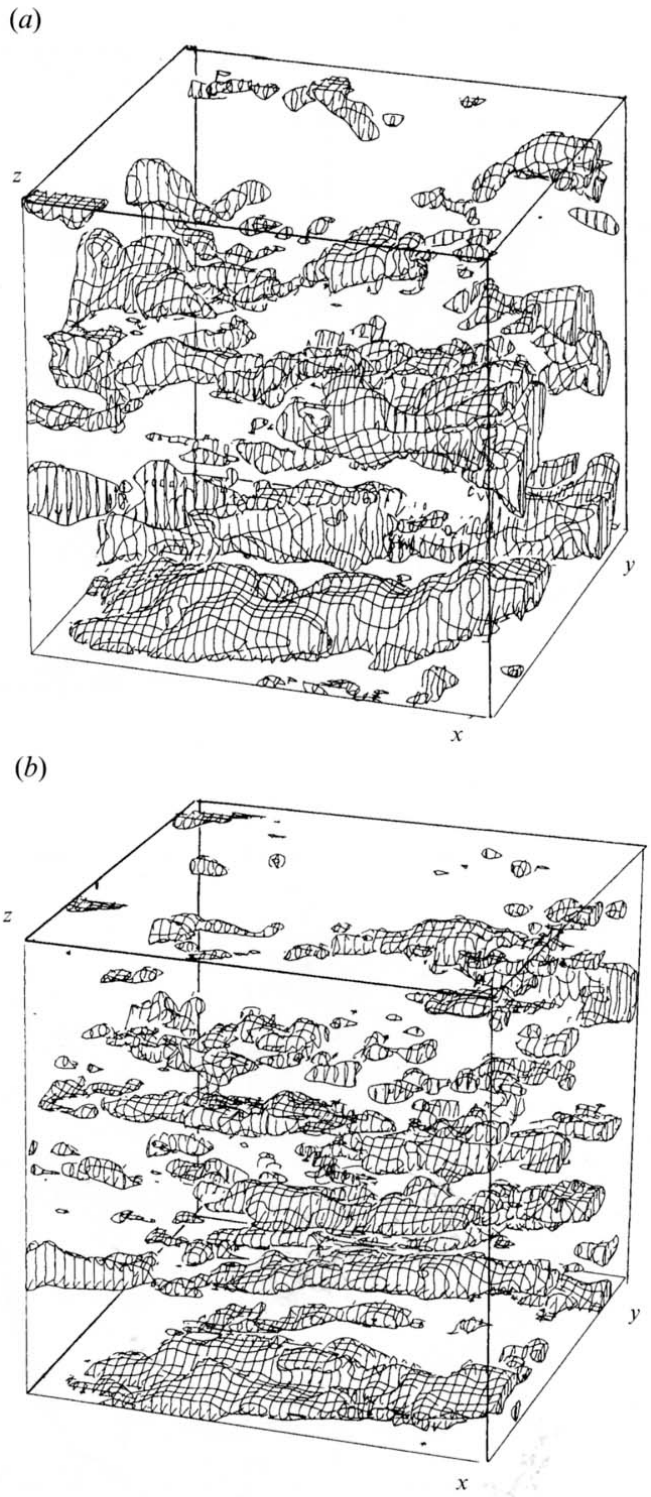

FIGURE 11. Perspective views of iso-surfaces of concentration fluctuation $c_1 \approx 1.3c_1'$ in a subdomain with side-lengths $\frac{1}{2}L$ at $St = 12$ for (*a*) $Ri = 0$, (*b*) $Ri = 0.5$. These results are from simulations with 96^3 grid points.

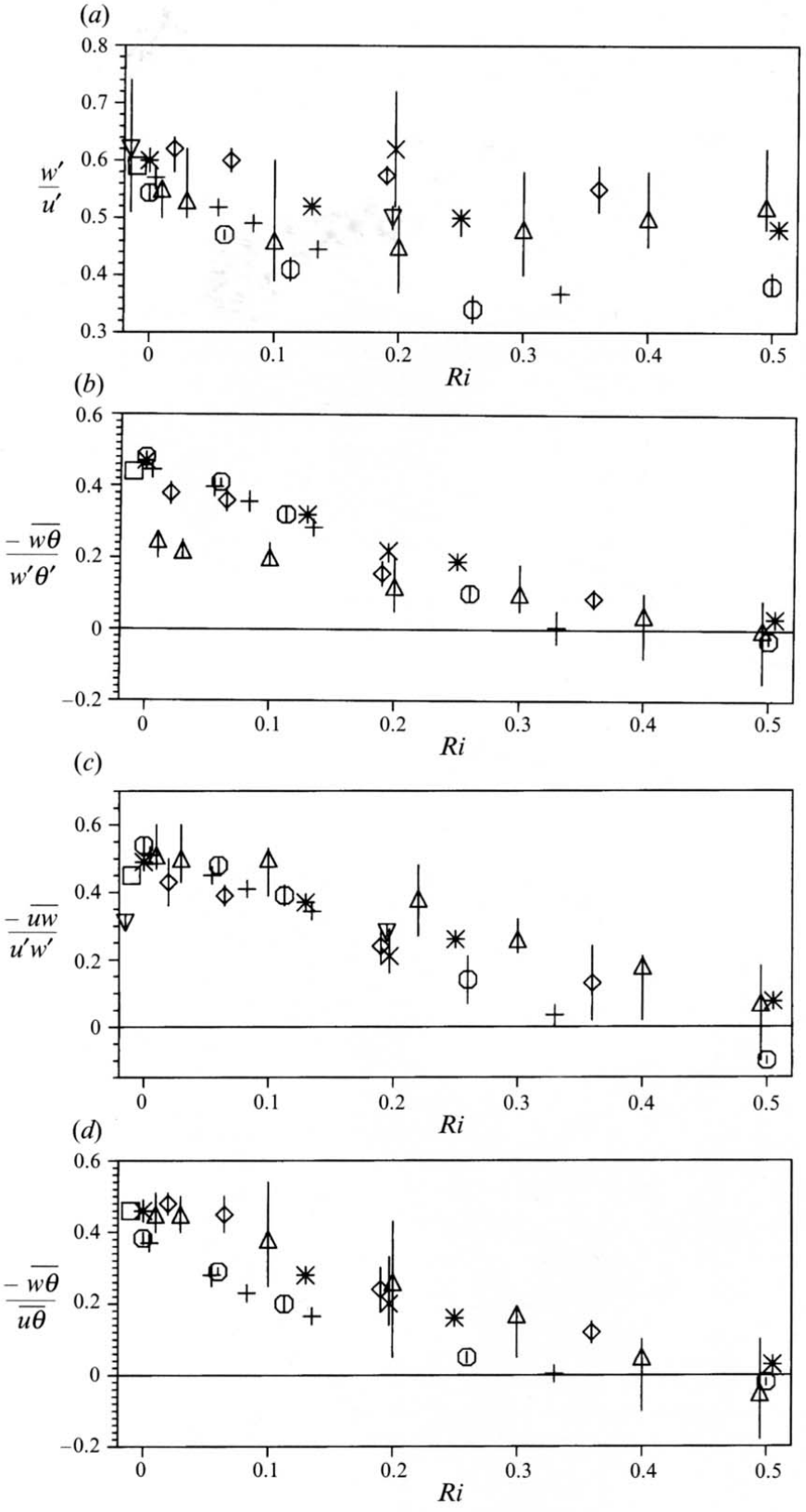

FIGURE 12. For caption see facing page.

$Ri = 0$ and 0.5. From similar plots of the velocity fields, we found, as in Gerz (1991) and Holt *et al.* (1992), that the shear motions form tubes of vortices when stratification is weak. These structures are inclined to the downstream direction by an angle of approximately 30°. The angle decreases and the tube-like vortices finally get destroyed when stratification becomes large. These dynamical structures also form the texture of species. At high stratification rather long downstream structures in the concentration fields prevail even when the vortex tubes have been destroyed. Hence, the structures of the concentration fields are built up by vortex dynamics at early times and persist when the motions have ceased.

3.3. *Comparison of simulation results with experimental data*

For neutral homogeneous shear flow, Tavoularis & Karnik (1989) summarized the state of knowledge with respect to the normalized Reynolds stress tensor as $K_{ij} = 0.51 \pm 0.04,\ 0.27 \pm 0.03,\ 0.22 \pm 0.02,\ -0.16 \pm 0.01$, for $ij = 11,\ 22,\ 33,\ 13$, respectively. The corresponding LES results are given in table 2. A reasonable estimate for the relative deviation between both data sets is expressed by $|(K_{ij})_{sim} - (K_{ij})_{exp}|/(\frac{1}{3}K_{ll})$, which is less than 12% at $St = 12$. Our neutral 96^3 simulations (LES and DNS, see Kaltenbach 1992), develop at $St = 12$ anisotropy levels which are 18% off in this sense. They show stronger temporal variation of K_{ij} than the 128^3 simulations; this is typical for low-Reynolds-number cases (cf. Roger *et al.* 1986). SGS contributions to the kinetic energy (see §3.5) amount to 14% of the resolved scale energy in the 128^3-LES and to 17% in the 96^3-LES. With SGS contributions, which are isotropic by definition, the numerical results agree even better with the measurements. For $Ri = 0$, Tavoularis & Karnik (1989) report a growth rate $F = 1.48 \pm 0.13$, which is close to our LES result 1.5 ± 0.05. Low-Reynolds-number DNS and coarse-grid LES deviate considerably from this value (see table 3). Only our fine-grid LES shows approximately equal growth rates for all three velocity variances as was observed by Tavoularis & Karnik (1989).

Figure 12 shows that the LES results agree quite well with data from a wide set of measurements and with previous numerical simulations (DNS). The scatter of data is quite large but small enough to allow some general conclusions. Before discussing the comparison, we describe briefly the various sources of data.

Rohr *et al.* (1988*b*) investigated homogeneous shear flow with stratification owing to variations of a salt concentration with height. The data are taken from the time period $5.7 < St < 9.6$ in this experiment. Homogeneous conditions were approximately achieved in Komori *et al.*'s (1983) investigation of channel flow of water heated at the top surface by condensing steam. The data plotted are those given by Komori *et al.* (1983) as best estimates. In the boundary-layer experiment of Morel *et al.* (1991) the stable stratification was induced by cooling a wind tunnel from below. Ri was approximately constant within the interval $0.3 < z/\delta < 0.57$ over which the averages are taken within the boundary layer of depth δ. Nieuwstadt (1984) measured turbulence characteristics within the nocturnal atmospheric boundary layer using a 200 m

FIGURE 12. Experimental data and simulation results versus Richardson number. The vertical bars denote the scatter of the data and the symbols denote the mean values from the laboratory experiments by ◇ Rohr *et al.* (1988*b*); △, Komori *et al.* (1983); ▽, Morel *et al.* (1991); □, Tavoularis & Corrsin (1981); ×, the atmospheric boundary layer observations by Nieuwstadt (1984); ○, the direct numerical simulations by Holt *et al.* (1992) and +, by Gerz & Schumann (1991); ✱, the present LES results. (*a*) Ratio of vertical to downstream r.m.s. velocity fluctuations, (*b*) correlation coefficient of negative vertical heat flux, (*c*) correlation coefficient of negative vertical momentum flux, (*d*) ratio of negative vertical to downstream heat flux.

high mast. The data show that Ri is close to 0.2 independent of height for a large range of altitudes in the stable layer. Here, we have plotted the mean values from his unfiltered data at altitudes large compared to the Obukhov length. In the wind-tunnel experiments of Tavoularis & Corrsin (1981, 1985) temperature acts as a passive scalar. We show mean values of measurements at $St = 8.6$, 10.9 and 12.7. Moreover, we compare time-averages of simulation data from the DNS of Holt *et al.* (1992) for $Re_\lambda = 52$ ($Re_l = 57$) and $Pr = 1$ at $St = 10$, 12 and 14, from the DNS of Gerz & Schumann (1991) for $Re_\lambda = 27$ and $Pr = 1$ in the interval $8 \leqslant St \leqslant 12$, and from our LES for $Pr_{SGS} = 1$ in the interval $8 \leqslant St \leqslant 12$.

As stated before, low-Reynolds-number DNS predict more anisotropic flows with smaller ratio w'/u' (figure 12*a*). The correlation coefficients of both the momentum and the heat flux decreases with Ri (figure 12*b*, *c*). The LES and the DNS give notably similar results for $Ri \leqslant 0.25$, but differ for $Ri = 0.5$. Despite the large Prandtl (Schmidt) number difference between salt water and air, experimental values of correlation coefficients agree quite well with each other and with the simulation results for Ri up to 0.25. Shear and stratification together also drive a downstream heat flux $\overline{u\theta}$ which becomes much larger than the vertical heat flux for strongly stratified flows (figure 12*d*).

The largest differences between the LES results and the bulk of experimental data are observed with respect to the boundary-layer data of Komori *et al.* (1983) and Morel *et al.* (1991). This indicates that these experiments do not behave as homogeneous turbulence. The rather close agreement between results from homogeneous flows and Nieuwstadt's (1984) data supports the local similarity hypothesis for the stable atmospheric boundary layer.

With respect to the lengthscales of turbulence, experimental data have been reported only for neutral shear flows. Tavoularis & Karnik (1989) found values for $S^2 l_{uu,x}^2/(-\overline{uw}) = 30 \pm 5$ in most of the relevant experiments. The LES reaches 29.6 at $St = 12$. Also the shear number $Sl_{uu,x}/q = 2.13$ is in good agreement with the experiment if we combine Tavoularis & Karnik's (1989) average values to obtain $(S^2 l_{uu,x}^2/(-\overline{uw})(-\overline{uw})/q^2)^{1/2} = (30 \times 0.16)^{1/2} = 2.2$. On the other hand, the shear number $Sl_{uu,x}/u' \approx 2.96$ of the neutral case underpredicts the values in between 3.6 and 4.0 reported by Rohr *et al.* (1988*a*) with no obvious reason.

Despite the high Prandtl-number difference, the data of Rohr *et al.* (1988*b*) and the LES and DNS results show similar variations of the energy ratio η with Ri. Measurements in the stably stratified boundary layer show much scatter, but lie lower than the simulation results. Nieuwstadt (1984) reports $\eta = 0.9 \pm 0.4$ for $Ri = 0.22 \pm 0.05$ while Hunt, Kaimal & Gaynor (1985) found values around $\eta \approx 0.64$ for $0.04 < Ri < 1$. These differences may be caused by the inhomogeneity of the boundary layer or by the influence of flow history (initial conditions) on the simulation results.

3.4. *Spectra*

3.4.1. *Variance spectra and spectral balances*

We have evaluated 'one-dimensional' spectra versus downstream, cross-stream (spanwise) and vertical wavenumbers (k_x, k_y, k_z, respectively) and also 'radial' spectra versus the spherical wavenumber $k = (k_x^2 + k_y^2 + k_z^2)^{1/2}$. Figure 13 shows such spectra of kinetic energy and temperature variance for LES with two different values of Pr_{SGS} and for three DNS. Most variance is gained at wavelengths in between $\frac{1}{6}$ and $\frac{1}{4}L$ and this corroborates our conclusion that the length-scale evolution is not influenced by the domain size. However, the variances at the first wavenumber are increasing, in particular for potential energy (or temperature variance) in strongly stratified flows, so

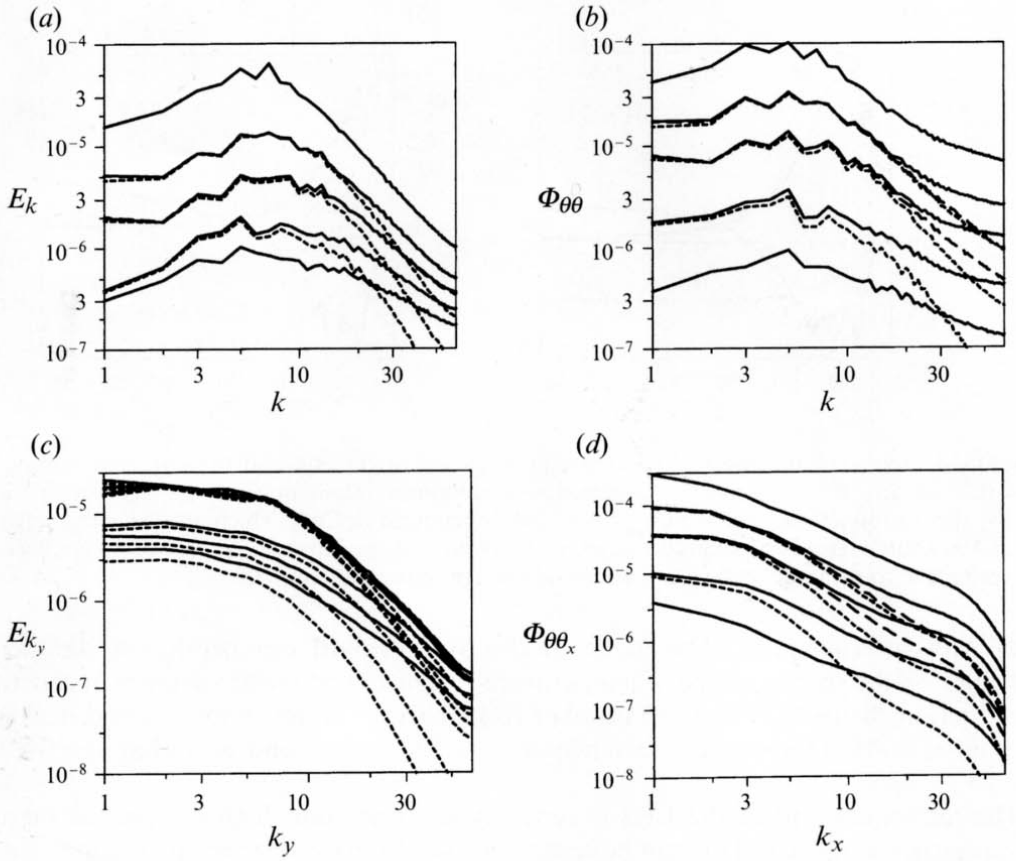

FIGURE 13. Power spectra versus radial wavenumber k of kinetic energy (a) and temperature variance (b) for $Ri = 0$, 0.13, 0.25, 0.5 and 1 (from top to bottom) at time $St = 11$. Power spectra versus cross-stream (k_y) wavenumber of kinetic energy for $Ri = 0.13$ and 0.5 at $St = 6$, 9 and 12 (c) and power spectra versus down-stream (k_x) wavenumber of temperature variance (d) as in (b). The full curves are from LES with $Pr_{SGS} = 1$, the long-dashed curves are from LES with $Pr_{SGS} = 0.5$ and the short-dashed curves from DNS. Spectral kinetic energy in units of $\Delta U^2 L$, spectral temperature variance in units of $\Delta\Theta^2 L$.

that the simulations could not be continued much longer with the fixed size of the computational domain.

The spectra of the LES are similar to those obtained from laboratory experiments with similarly restricted ranges of scales. Rohr *et al.*'s (1988*b*) spectra of horizontal velocity versus frequency (downstream wavenumber) also have negative slopes in an intermediate wavenumber range lying between about 2 for $Ri = 0$ and about 1.5 for $Ri = 0.37$. The negative slopes generally decreases when Ri grows.

Figure 13(*c*) shows cross-stream spectra of kinetic energy for several times. Spectra of LES develop time-independent shapes whereas all supercritical DNS develop progressively steeper slopes at the high-wavenumber end as time proceeds. However, even at late times ($St = 11$), low wavenumbers contain similar amounts of energy in LES and DNS. Differences in the evolution of the integral lengthscale between LES and DNS are therefore not caused by changes at large scales but are due to changes in the spectral shape (cf. figure 7).

We observe similar trends in the temperature-variance spectra (figure 13*b*, *d*): much more potential energy remains available at intermediate and high wavenumbers of LES cases than of DNS cases. Radial spectra of temperature variance tend to be flatter in

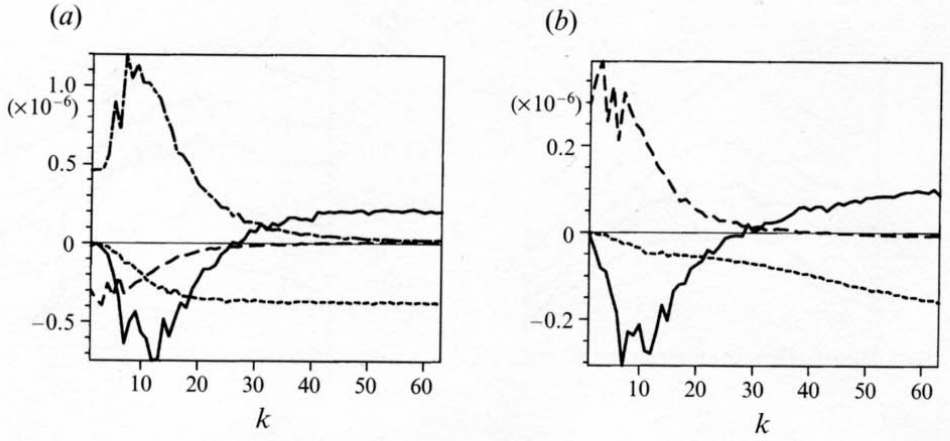

FIGURE 14. Terms of the spectral balance equations for (*a*) kinetic and (*b*) potential energy for $Ri = 0.25$ at $St = 8$; ——, energy transfer due to nonlinear interactions; ---, energy dissipation; —·—, shear production term $-SCo_{uw}$; – – –, buoyancy term $\beta g Co_{w\theta}$, which acts as energy sink in (*a*) and as source term for potential energy in (*b*). Note that the balances are not complete because the terms due to mean advection and temporal change have been omitted.

LES with increasing Ri. The value of the SGS-Prandtl number has a significant influence on the spectral slope of temperature variance (and scalar variance in general). A reduction of the SGS-Prandtl number from 1 to 0.5 causes a more rapid decay of one-dimensional temperature variance spectra for $k_x > 5$ and of radial spectra for $k > 15$.

The numerical grid of the LES is certainly not fine enough to resolve the inertial subrange of turbulence. This can be seen from the shape of the spectra in figure 13 and is even more obvious from the transfer spectra in figure 14 which do not vanish for a band of wavenumbers. From figures 13(*a*) and 13(*c*) for $Ri = 0$ we find the power law of k^{-2}. This is consistent with the rapid distortion analysis of Hunt & Carruthers (1990). However, the fact that the energy spectra in the LES (and also in Rohr's measurements) decrease less steeply for large Richardson numbers than for neutral flow deviates from general expectations (Monin & Ozmidov 1985). One possible explanation is that the vertical heat flux is most efficient at small and moderate wavenumbers thus reducing kinetic energy in these simulations, see curve of $\beta g Co_{w\theta}$ in figure 14. This would be consistent with Stillinger *et al.* (1983) and Itsweire *et al.* (1986) who report spectra of vertical velocity fluctuations where the large scales are suppressed first by stable stratification while smaller scales remain energetic. On the other hand, plots of various terms of spectral balances for kinetic and potential energy (figure 14) reveal that for $k > 30$, the dissipation rates form the most important contribution to the local wavenumber budgets and, therefore, determine the slope of the energy spectra. These terms strongly depend on the SGS-model which, therefore, controls the spectral slope near the cutoff wavenumber. Because of the uncertainty introduced by the SGS-model, we regard our series of simulations as representing upper and lower bounds for possible flow evolutions in a qualitative sense and not in an exact quantitative sense.

3.4.2. *Co-spectra of shear stress and vertical heat flux*

Since shear and stratification create anisotropic structures in the flow we expect that this information is also reflected in directional co-spectra of vertical fluxes of momentum and heat. In particular, the question of which scales of motion contribute

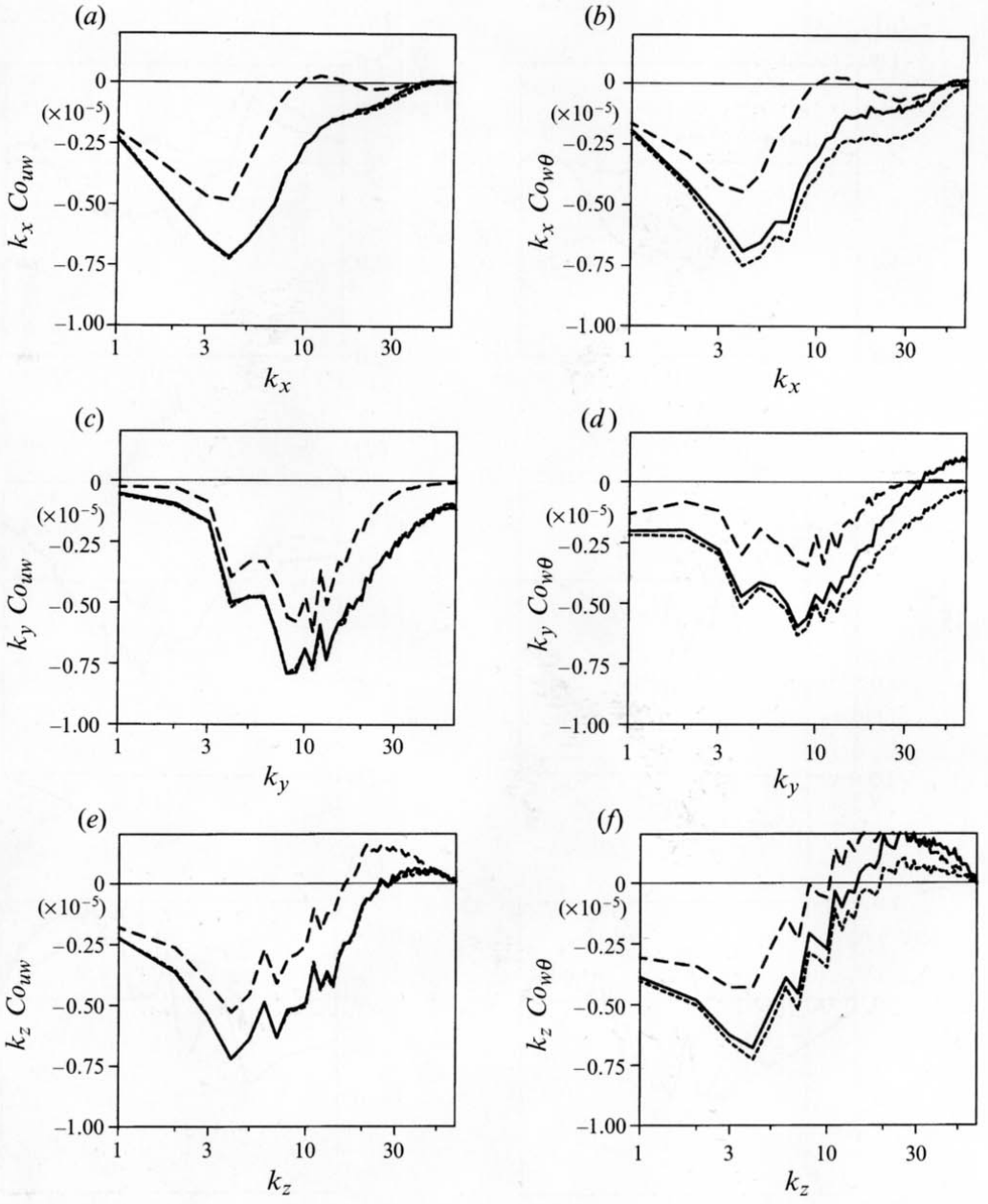

FIGURE 15. Co-spectra for momentum (a, c, e) and vertical heat flux (b, d, f) versus k_x, k_y, k_z in variance preserving form for $Ri = 0.25$ at $St = 11$. ——, LES ($Pr_{SGS} = 1$); ----, LES ($Pr_{SGS} = 0.5$); – – –, DNS.

to positive, i.e. counter-gradient, fluxes at strong stratification can be answered in greater detail by analysing one-dimensional spectra. Previous DNS work (Gerz & Schumann 1991; Holt *et al.* 1992) analysed the fluxes on the basis of radial co-spectra only. We examine co-spectra of uw and $w\theta$ versus k_x, k_y and k_z in a variance preserving form, i.e. $k_i Co(k_i)$ versus $\log k_i$. We choose the two cases with $Ri = 0.25$ (figure 15) and $Ri = 0.5$ (figure 16) as representatives for a moderately stratified flow and a more strongly stratified flow at developed stages, $St = 11$. LES and DNS results are depicted. Figure 15 also shows the influence of varying SGS-Prandtl number.

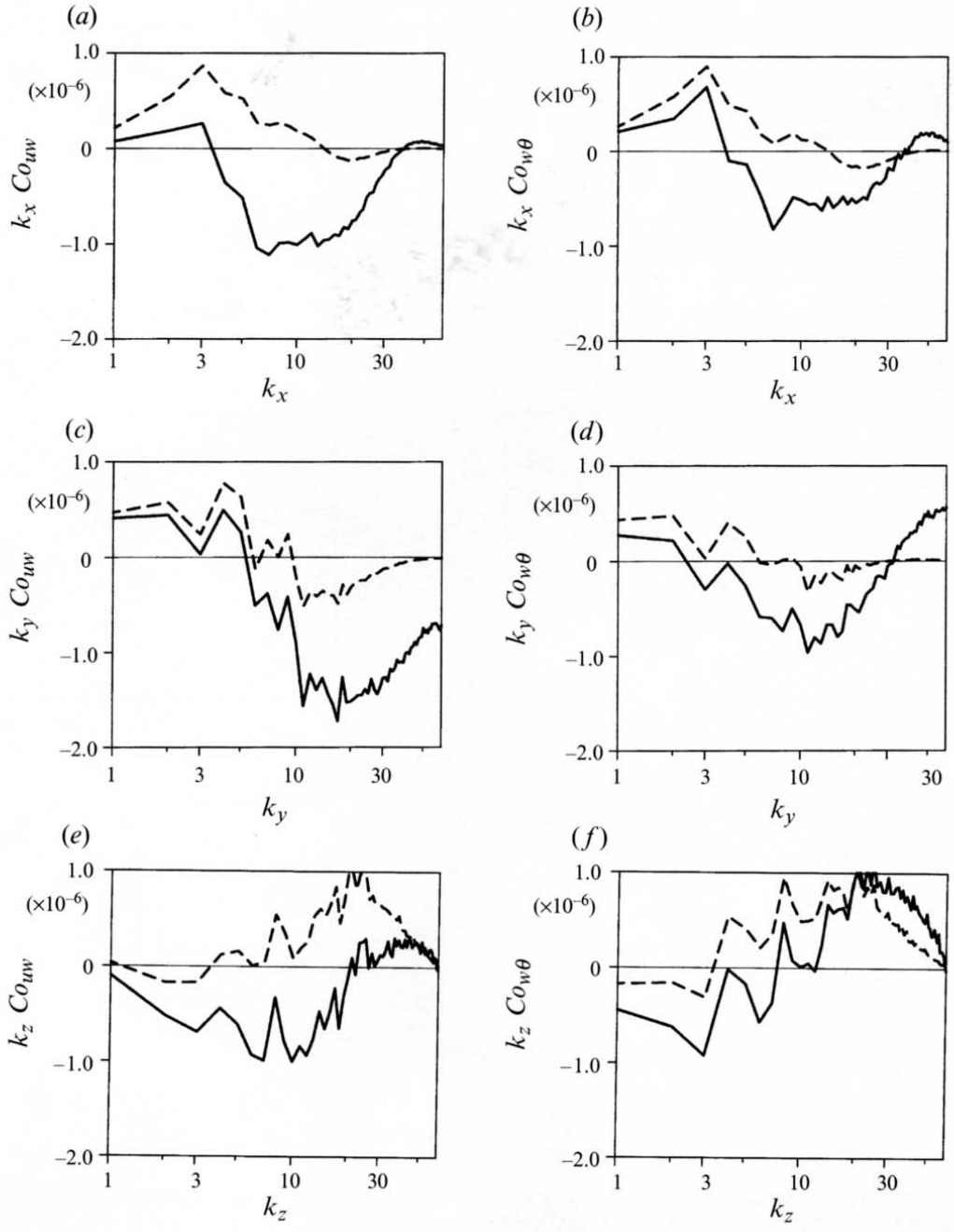

FIGURE 16. As in figure 15 for $Ri = 0.5$ and $Pr = 1$.

In general, the shape of a co-spectrum differs drastically with respect to the direction of the Fourier transform. Therefore, radial cospectra may be misleading. Differences are found at large and small scales. The DNS data differ from LES data, in particular at $Ri = 0.5$. Since turbulence decays at larger rates in the DNS than in the LES, the fluxes in DNS are generally smaller at all wavenumbers, except for the small-scale counter-gradient contributions in the vertical co-spectra. In accordance with the reports of Holt *et al.* (1992), examination of phase relations between w and θ does not reveal the presence of significant (linear) wave motion at the late flow stage (cf. Kaltenbach 1992).

When $Ri = 0.25$, the large and intermediate scales contribute most to the down-gradient fluxes of momentum and heat. The spanwise wavenumber at which the strongest fluxes occur corresponds to the peak in the energy spectrum of the initial velocity field. Hence, the mean shear does not change the mean spanwise spacing of structures that cause intense fluxes. Conversely, both downstream and vertical co-spectra peak at smaller wavenumbers indicating that structures are elongated in the streamwise and vertical direction. The fluxes essentially vanish at small scales with respect to the horizontal directions. At small scales with respect to k_z, however, significant counter-gradient fluxes for momentum and heat appear in LES and DNS. The heat flux at high wavenumbers is strongly sensitive to the value of Pr_{SGS}, the shear stress is not. Hence, at moderate Richardson numbers, the flow dynamics (represented by the shear stress) are rather insensitive at all scales to the value of the SGS-Prandtl number.

For $Ri = 0.5$, the averaged turbulent vertical fluxes of heat and momentum become persistently counter-gradient in the DNS at times $St > 9$ whereas these fluxes remain down-gradient in the corresponding LES. At early times ($St < 3$), the flux co-spectra for $Ri = 0.5$ look similar to those shown for $Ri = 0.25$. When $4 < St < 9$, the fluxes for $Ri = 0.5$ change sign at low wavenumbers and thus reflect the periodic exchange of potential and kinetic energy which also causes the oscillating parts of the timeseries of $\overline{uw}$ and $\overline{w\theta}$. When $St > 10$, the co-spectra do not change shape until the end of simulation ($St = 12$).

Figure 16 reveals that horizontal co-spectra of both LES and DNS at $St = 11$ have counter-gradient contributions at large scales and negative values in the medium wavenumber range. The down-gradient fluxes at intermediate wavenumbers are much stronger in the LES than in the DNS. Fluxes vanish at high (horizontal) wavenumbers in the DNS but become counter-gradient again in the LES (except for $Co_{uw}(k_y)$). On the other hand, vertical co-spectra show vanishing or down-gradient fluxes at low wavenumbers and rather strong positive contributions at intermediate and small scales in LES and DNS. These observations are also made in the LES with $Ri = 1$ (cf. Kaltenbach 1992) where the fluxes at low horizontal wavenumbers as well as the average fluxes remain persistently counter-gradient for more than one buoyancy period.

The flux co-spectra measured in the horizontal directions show that strong stratification influences sheared turbulence in roughly the same way as shear-free turbulence. Lienhard & Van Atta (1990) and Yoon & Warhaft (1990) found in their shear-free stratified wind-tunnel experiments that buoyancy modifies the co-spectra mostly at low wavenumbers, which periodically change their sign, whereas the fluxes at smaller scales remain down-gradient for a long time. The rather weak fluxes at low vertical wavenumbers reflect the fact that buoyancy suppresses vertical motion most efficiently on large scales which have large turnover times (and therefore high values of Fi) and forces the flow into thin horizontal layers (Métais & Herring 1989). From the general similarity of the co-spectral shapes of heat and momentum fluxes in flows with $Ri = 0.25$ and $Ri = 0.5$ it is most likely that both fluxes stem mainly from the same dynamical large-scale processes, which is one of Prandtl's basic hypotheses. Differences between Co_{uw} and $Co_{w\theta}$ are most obvious at the smallest scales (especially pronounced for $Ri = 0.5$).

Previous analysis based on the radial co-spectra from DNS stated that timely persistent counter-gradient fluxes are caused by small scales whereas the large scales are responsible for periodic contributions to the time series of vertical fluxes (Gerz & Schumann 1991). Our one-dimensional co-spectra give a more complex picture. The

horizontal co-spectra indicate that the largest amount of counter-gradient fluxes stems from the large scales.

In particular in the DNS at $Ri = 0.5$, where mean fluxes become positive at late times, we find the strongest counter-gradient contributions in the horizontal flux co-spectra at low wavenumbers. The counter-gradient fluxes at these scales originate from the strong mixing in the initial period and, hence, are a consequence of flow history. Therefore, large-scale counter-gradient fluxes do not represent an asymptotic or self-similar flow state and this phenomenon should not be restricted to low Reynolds numbers. Conversely, the vertical co-spectra exhibit the counter-gradient flux phenomenon predominantly at small scales where the heat flux strongly depends on the Prandtl number. Possible explanations for small-scale flux reversal are given in Schumann (1987), Holloway (1988), Gerz *et al.* (1989), Kaltenbach, Gerz & Schumann (1991), Gerz & Schumann (1991), Holt *et al.* (1992) and Gerz (1993).

The differences between LES and DNS with respect to counter-gradient fluxes may originate from the different mixing at medium wavenumbers or from differences in the dissipation regime. For $Ri = 0.5$ we find that the medium wavenumbers of the LES are much more energetic than in the DNS. Because these wavenumbers are less influenced by buoyancy than the large scales they continue to mix temperature or momentum down-gradient, which causes the overall fluxes to remain more negative in the LES than in the DNS. On the other hand, if counter-gradient fluxes are due to dissipative processes at small scales, they will depend on details of the SGS model (like Pr_{SGS}).

It is noteworthy that the LES partly produces stronger counter-gradient fluxes at small scales in the more energetic flow than the respective DNS in the less energetic flow. Finally, one should not overlook the fact that the average fluxes for $Ri \geqslant 0.5$ become small at late times anyway, and typically stay below 1% of the maximum values in the initial period.

3.5. *Influence of the SGS-model and the grid resolution*

Large-eddy simulations rely on the hypothesis that the results depend only weakly on grid resolution and the details of the SGS model as long as it provides the correct amount of dissipation. Lilly (1967) showed that the coefficient c_{SGS} can be evaluated from the inertial range theory of turbulence when the grid scale is small enough such that the smallest resolved scales represent locally isotropic turbulence with an energy spectrum $E(k) = \alpha\epsilon^{2/3}k^{-5/3}$. For a Kolmogorov coefficient of $\alpha = 1.6$ this results in $c_{SGS} = 0.17$ (Schmidt & Schumann 1989).

Our simulations lack an inertial subrange which can hardly be obtained unless the resolution is much finer than we were able to provide. A common practice in LES of a wide variety of flows is to account for the lack of an inertial subrange by adjusting c_{SGS} in such a manner that energy is dissipated at a sufficient rate. Other SGS models like the structure function model of Métais & Lesieur (1992) suffer basically from the same problem. Germano *et al.* (1991) developed a procedure to determine c_{SGS} dynamically during the simulation by measuring energy transfer rates close to the wavenumber cutoff. This is particularly important in inhomogeneous flows where c_{SGS} may vary with the location. The spatial variability of c_{SGS} is of minor importance in homogeneous turbulence where good results may be obtained with a fixed value of c_{SGS}. However, the ability of the dynamic model to adapt c_{SGS} to temporal changing flow conditions might be of particular interest in stratified flows which undergo significant changes in time. As explained in the next paragraph our modified version of the Smagorinsky model has some dynamical or self-adapting features. We do not expect, therefore, significantly different LES results when applying the dynamic model.

However, a detailed comparison of various SGS-models in stratified turbulence is desirable but beyond the reach of the present work.

LES of channel flow using the dynamic model shows that c_{SGS} is smaller in regions with high mean shear in the vicinity of walls compared to zones with weaker shear in the centre of the channel. This is consistent with findings of Schumann (1975) and Rogallo & Moin (1984) who stated that the value of c_{SGS} tends to be more universal when the mean velocity gradient is removed before computing the strain rate magnitude. Moin *et al.* (1991) found values for c_{SGS} between 0.06 and 0.08 from *a priori* tests of DNS data of homogeneous shear flow, i.e. more than 50% smaller than the theoretical value for inertial range turbulence of 0.17. For the present LES we find that the ratio of average local deformation magnitude $(2S_{ij}S_{ji})^{1/2}$ (computed without mean shear S) and mean shear S is close to one with the tendency to smaller values when Ri is increasing. We therefore decided to remove the mean shear from the computation of S_{ij} which has several advantages: first, this allows us to use the theoretical value $c_{SGS} = 0.17$ which does not have to be modified owing to the presence of shear. Including S in the computation of the strain rate would require an empirical reduction of c_{SGS} by approximately 50% in order to recover good agreement of the growth rate F with experiments of homogeneous neutral shear flow. Secondly, one strong feature of our LES, namely the self-adaptation of the SGS-model to changing flow conditions, would be severely reduced, especially in the cases with $Ri \geqslant 0.5$, because inclusion of S in the strain rate acts like adding a timely constant viscosity. Because the mean shear becomes stronger than the (average) local strain rate magnitude (computed without the mean shear) in strongly stratified cases, the major part of the SGS-stresses would simply be deterministic like in a DNS. Moreover, severe problems of a constant viscosity type SGS-model are to be expected in strongly stratified cases which may be close to relaminarization. Our model for ν_t has the desirable property of vanishing in a shear flow which relaminarizes owing to stratification effects.

Mason & Derbyshire (1990) applied a model in which the SGS diffusivities get reduced in regions where the local stratification increases. This has effects similar to reducing the value of c_{SGS}. Since the mean temperature gradient s has the same order of magnitude as the fluctuating temperature gradients $(\partial\theta/\partial z)'$, the percentage Υ of locally convective regions becomes very small for $Ri \geqslant 0.5$. Therefore, at almost all locations c_{SGS} is reduced when one accounts for the influence of stability. As a consequence we found that the model causes large energy and variance at small scales (Kaltenbach 1992). Hence, we do not include the effect of stratification in our SGS model. Stratification should only be considered when the deformation rate includes the mean shear because in this case it is certainly desirable to have a mechanism which reduces the dissipative properties of the model when Ri increases.

As a further argument for this decision we consider the magnitude of shear and buoyancy for the SGS motions. Relevant measures are the SGS shear number $Sh_{SGS} = S\Delta x/(2e)^{1/2}$ and the related inverse Froude number, $Fi_{SGS} = Sh_{SGS}\,Ri^{1/2}$. In the inertial range, the SGS kinetic energy e can be estimated from $e = (\nu_t/(c_\nu \Delta x))^2$, where $c_\nu = 0.0856$ (Schmidt & Schumann 1989). Sh_{SGS} and Fi_{SGS} should be small in order to justify the assumption of locally isotropic turbulence at the smallest resolved scales of the LES. However, as shown in figure 9(*a*), Sh_{SGS} is of order unity. Since $\epsilon \sim e^{3/2}/\Delta x$, the SGS shear number scales with $\Delta x^{4/3}$ for fixed dissipation rate, an assumption which is only approximately satisfied. A reduction of Sh_{SGS} by a factor of ten would be desirable, but would require $10^{3/4} \approx 5.6$ times more grid point in each coordinate direction. Since $Fi_{SGS} \leqslant Sh_{SGS}$ for $Ri \leqslant 1$, the impact of buoyancy forces

on SGS motions is of smaller importance than the impact of mean shear. Therefore, any changes of the SGS diffusivities as a function of local stability are of minor relevance compared to the impact of shear.

The theory of locally isotropic inertial-range turbulence also suggests a SGS Prandtl number of about 0.5 (Schmidt & Schumann 1989), but this value should rise under strong stratification (Schumann 1991). Partly for this reason, but mainly for comparisons with DNS of fluid flows with $Pr = 1$, we used $Pr_{SGS} = 1$ for the basic set of the LES cases. The data presented for $Pr_{SGS} = 0.5$, see table 2, show that most results (in particular the flow dynamics at $Ri \leqslant 0.25$ in terms of quantities such as K_{ij}, F, and $\overline{uw}/(u'w')$) depend only a little on this Prandtl number. Larger sensitivity is found for strong stratification and for quantities that depend on the strength of scalar fluctuations such as $\overline{w\theta}/(w'\theta')$, Pr_t, and η. This sensitivity is to be expected and remains an unavoidable source of uncertainty for the present study. Fortunately, scalar flux ratios like $\overline{w\theta}/\overline{u\theta}$ and D_{ij}/D_{22} (see §4.2) depend only a little on Pr_{SGS}.

The suitability of our SGS model is supported by reasonable spectral shapes, as discussed in §3.4, and by the fact that the growth rate P/ϵ for neutral shear flow is computed in excellent agreement with the experimental data.

From the values presented in table 3 we derive some conclusions concerning the sensitivity of results with respect to grid resolution. We find that in the weakly stratified cases with $Ri \leqslant 0.13$, differences between an LES and a DNS which were carried out on the same grid (and with comparable effective Reynolds numbers) are less pronounced than differences between fine-grid simulations (128^3) and coarse-grid simulations (96^3) of the same type (cf. figure 5*b* for $Ri = 0$). We find anisotropy levels $K_{ij} - \frac{1}{3}\delta_{ij}$ which are in average 15% higher in the coarse-grid LES than in the fine-grid LES. This changes most other quantities like diffusive properties in the range of 10–20%. Because the LESs show a similar trend with respect to grid resolution as the DNSs (see §3.2), we conclude that differences in the dissipation at small scales and the resultant changes in the transfer rates from large to small scales determine the level of anisotropy. Obviously, the effective Reynolds number of the LES is not yet high enough for the flow to become independent on this parameter. Nevertheless, for $Ri = 0$, our fine-grid LES results agree significantly better with experimental data than the coarse-grid results.

In decaying stratified flows, i.e. for $Ri \geqslant 0.25$, LES and DNS results differ considerably whereas the differences between coarse-grid and fine-grid simulations are relatively small. For example, both LES produce average down-gradient fluxes at $Ri = 0.5$, whereas both respective DNS become counter-gradient. We explain this with the increasing importance of the Froude number as a flow-controlling parameter when stratification increases. Whereas Fi of DNS and LES evolve very differently on both fine and coarse grids, the effect of grid resolution on Fi for the same simulation type is rather small (Fi of the coarse grid cases are given in Kaltenbach 1992).

In conclusion we find that the SGS-model gives consistent results in neutral as well as stratified turbulence without the need to adjust the model parameters to a specific situation. The sensitivity due to grid resolution is partly related to changes in the effective Reynolds number.

4. Turbulent diffusion

4.1. *Results*

An often used approximation in the modelling of turbulent diffusion is based on the assumption that turbulent fluxes can be linearly related to gradients of the mean value

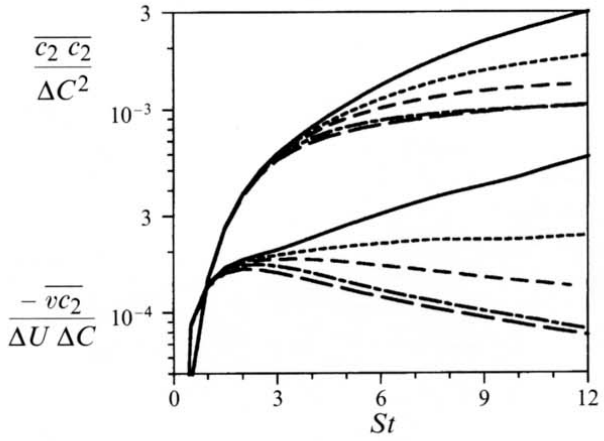

FIGURE 17. Species-concentration variance (upper curves) and negative fluxes (lower curves) induced by a cross-stream gradient versus shear time for LES cases with different Richardson numbers. Line coding as in figure 2.

of the transported quantities. It has long been known that such a relationship is often wrong in principle (because other forces may contribute to fluxes or when the principle of scale-separation is violated), yet can be useful in practice (Corrsin 1974). In general, the fluxes and gradients are related by a second-rank 'turbulent diffusivity tensor',

$$\overline{u_i c} = -D_{ij}\frac{\mathrm{d}C}{\mathrm{d}x_j}. \tag{6}$$

The components D_{ij} can be 'measured' in terms of the fluxes induced by three independent concentration fields C_i with uniform gradients s_i in the three Cartesian directions. Because of flow symmetry only five out of nine tensor components are different from zero.

The down-gradient flux $\overline{vc}_2$ is shown in figure 17. Evolution of the vertical and horizontal heat fluxes, i.e. $\overline{w\theta}$ and $\overline{u\theta}$, from which the tensor components D_{33} and D_{13} are gained, was presented in previous sections. The downstream flux $\overline{uc}_1$ develops in a similar manner as the cross-stream flux $\overline{vc}_2$. Both fluxes evolve similarly as the kinetic energy. They grow for $Ri = 0$, become stationary for $Ri = 0.13$ and decay for $Ri \geqslant 0.25$. Unlike the vertical scalar flux $\overline{w\theta}$, none of the horizontal fluxes becomes zero or changes its direction.

We find a large difference in the temporal development of the variance $\overline{\theta^2}$ compared to that of the scalar variances $\overline{c_1^2}$ and $\overline{c_2^2}$. Whereas $\overline{\theta^2}$ diminishes significantly for $Ri > 0.13$ (see $E_{pot} \sim \overline{\theta^2}$ in figure 2*b*), both other variances grow in time for all Ri (figure 17). The corresponding correlation coefficients of the horizontal fluxes reach stationary values in between 0.6 and 0.7, which are relatively independent of Ri (table 2).

In order to measure the degree of anisotropy of the turbulent diffusion process, we normalize the tensor components with the spanwise diffusivity D_{22}. Normalization by D_{33} as in Rogers *et al.* (1989) is not applicable because of vanishing vertical heat flux for strong stratification. For all Ri, all tensor-component ratios D_{ij}/D_{22} reach approximately steady values in the interval $6 < St < 12$, see figure 18. The curves D_{11}/D_{22} show a slight trend with time towards higher values which is closely related to a similar trend in the ratio $\overline{u^2}/\overline{v^2}$. DNS develop similar ratios D_{ij}/D_{22} as LES, indicating that the anisotropy of scalar transport properties depends only weakly on the small-scale motions.

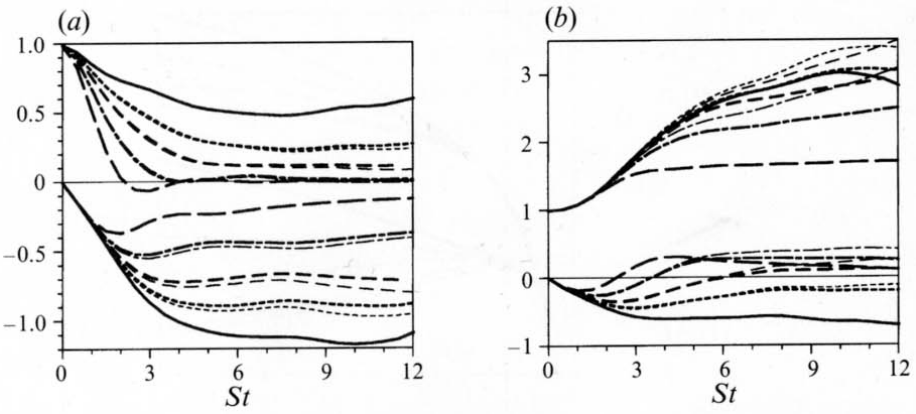

FIGURE 18. Normalized diffusivity tensor components versus St. (a) D_{33}/D_{22} (upper curves) and D_{13}/D_{22} (lower curves); (b) D_{11}/D_{22} (upper curves) and D_{31}/D_{22} (lower curves). Line coding as in figure 2.

4.2. *Discussion of scalar transport properties*

For understanding, it is useful to consider the transport equations for the non-vanishing fluxes,

$$-D_{11}: \quad \partial\overline{uc}_1/\partial t = -\overline{uu}s_1 - \overline{wc}_1 S + \phi_{1c_1} - \epsilon_{1c_1}, \tag{7}$$

$$-D_{31}: \quad \partial\overline{wc}_1/\partial t = -\overline{uw}s_1 + \beta g\overline{\theta c}_1 + \phi_{3c_1} - \epsilon_{3c_1}, \tag{8}$$

$$-D_{22}: \quad \partial\overline{vc}_2/\partial t = -\overline{vv}s_2 + \phi_{2c_2} - \epsilon_{2c_2}, \tag{9}$$

$$-D_{13}: \quad \partial\overline{uc}_3/\partial t = -\overline{uw}s_3 - \overline{wc}_3 S + \phi_{1c_3} - \epsilon_{1c_3}, \tag{10}$$

$$-D_{33}: \quad \partial\overline{wc}_3/\partial t = -\overline{ww}s_3 + \beta g\overline{\theta c}_3 + \phi_{3c_3} - \epsilon_{3c_3}, \tag{11}$$

$$\partial\overline{\theta c}_1/\partial t = -\overline{u\theta}s_1 - \overline{wc}_1 s - \epsilon_{\theta c_1}, \tag{12}$$

$$\partial\overline{\theta c}_3/\partial t = -\overline{w\theta}s_3 - \overline{wc}_3 s - \epsilon_{\theta c_3}, \tag{13}$$

$$\partial\overline{c_1^2}/\partial t = -2\overline{uc}_1 s_1 - \epsilon_{c_1}, \tag{14}$$

$$\partial\overline{c_2^2}/\partial t = -2\overline{vc}_2 s_2 - \epsilon_{c_2}, \tag{15}$$

with related pressure correlations ϕ and dissipation rates ϵ. Note the formal equivalence of c_3 and θ.

A simple approximation for the sink terms, used e.g. by Yamada (1977), Freeman (1977), and Rogers *et al.* (1989) assumes

$$\phi_{ic_j} - \epsilon_{ic_j} = -\overline{u_i c_j}/\tau_{mod}, \tag{16}$$

with a suitable timescale $\tau_{mod} = c_c q^2/\epsilon$ and a constant coefficient c_c of the order one. Others have assumed more complicated relationships with extra terms describing linear interactions between the mean gradients and the turbulence fluctuations due to pressure forces (Launder 1978; Tsarenko 1989), and with c_c depending on shear time and Reynolds number (Rogers *et al.* 1989). However, the simple relationship suffices to explain the basic effects. If one assumes, moreover, steady state in the sense $\partial\overline{u_i c_j}/\partial t \ll \overline{u_i c_j}/\tau_{mod}$, one obtains an implicit expression for the diffusivities

$$D_{ij} = \tau_{mod} \begin{bmatrix} \overline{uu} + \overline{wc}_1 S/s_1 & 0 & \overline{uw} + \overline{wc}_3 S/s_3 \\ 0 & \overline{vv} & 0 \\ \overline{uw} - \overline{\theta c}_1 \beta g/s_1 & 0 & \overline{ww} - \overline{\theta c}_3 \beta g/s_3 \end{bmatrix}. \tag{17}$$

Similarly, one obtains estimates for the cross-correlations $\overline{\theta c}_1$ and $\overline{\theta c}_3 = \overline{\theta\theta}s_3/s$. These approximations result in a linear system of equations for the tensor components D_{ij}. Equation (17) is identical with Rogers *et al.*'s (1989) model for D_{ij} when the fluxes $\overline{wc}_1$ and $\overline{wc}_3$ are expressed in terms of the corresponding modelled coefficients D_{31} and D_{33}.

For positive mean gradients and weakly stratified flows, one can deduce from (25), (27) and (26) that $\overline{uw} < 0$, $\overline{w\theta} < 0$, $\overline{u\theta} > 0$. Hence, the above equations yield $\overline{wc}_1 > 0$, $\overline{\theta c}_1 < 0$, $\overline{\theta c}_3 > 0$, and $\overline{wc}_3 < 0$. As a consequence, the relations $D_{11} > \overline{uu}\tau_{mod}$, $D_{22} = \overline{vv}\tau_{mod}$, $D_{33} < \overline{ww}\tau_{mod}$, $D_{13} < \overline{uw}\tau_{mod} < 0$, and $D_{31} > D_{13}$ follow. The component D_{31} is negative for strong shear but may change sign and become positive for strong stratification. Also D_{33} may change sign and become negative. The diffusivity tensor is symmetric only for isotropic turbulence but asymmetric is sheared and in stratified turbulence. This asymmetry is a fundamental difference to molecular diffusion processes.

The differences in the temporal development of the scalar variances $\overline{c_1^2}$, $\overline{c_2^2}$ and $\overline{c_3^2} \sim \overline{\theta^2}$ stem from the different source terms which generate these variances. Buoyancy forces connect the vertical flux $\overline{wc}_3 \sim \overline{w\theta}$ and the corresponding variance $\overline{\theta^2}$ (see (27) and (28)) which limits the growth of temperature variance at strong stratification. There is no such buoyancy coupling between the horizontal fluxes $\overline{uc}_1$ and $\overline{vc}_2$ (see (7) and (9)) and the corresponding variances (see (14) and (15)).

The correlation $\overline{\theta c}_1$ is important for the diffusivity component D_{31} in stratified flows (see (17)). The corresponding correlation coefficient reaches a rather large value of -0.74 in a neutral flow (table 2). Rogers *et al.* (1989) conclude from the high correlation of θ and c_1 that the concentration fields quickly adjust to the velocity field. The strong decrease of $\overline{\theta c}_1/(\theta' c_1')$ under strong stratification indicates a decoupling of horizontal and vertical motion. The quick decay of the shear stress corroborates this view. This correlation coefficient $\overline{\theta c}_1/(\theta' c_1')$ reaches stationary values very slowly in cases with $Ri \geqslant 0.5$. These data do not collapse as well as others when plotted against Fi (figure 10). This might indicate that flow history affects species concentrations more than dynamics (see also figure 11).

Mean values of D_{ij}/D_{22} for different Ri are represented in table 2 and in figure 19. Figure 19 contains also the results obtained by Rogers *et al.* (1989) from DNS for neutral shear flow (data taken from Rogers *et al.* 1986) and measurements of Tavoularis & Corrsin (1981, 1985). For neutral flows, the simulations agree in the sense that D_{11} is about three times larger than D_{22}, and D_{33} is roughly half the value of D_{22}. As expected from (17), this ratio is larger than that of the velocity variances, which equals 1.74:1:0.6 in the LES (1.71:1:0.84 in the DNS of Rogers *et al.* 1989). Both off-diagonal components are negative and $D_{13} < D_{31} < 0$, as expected. Tavoularis & Corrsin (1981, 1985) measured $D_{13}/D_{22} = -1.4$, $D_{33}/D_{22} = 0.63$, whereas the LES gives $D_{13}/D_{22} = -1.10$, $D_{33}/D_{22} = 0.52$, for $Ri = 0$.

The theory leading to (17) assumes that the timescale τ_{mod} is the same for all correlation components. Dörnbrack (1991) applied a more complete theory based on the SOC closure deduced by Yamada (1977) which results in (17) and he provides an explicit approximation for τ_{mod} as a function of l/q. Figure 19 shows the results of this model which are obtained if the Reynolds stresses are taken from the LES. For $Ri = 0$, this results in $D_{ij}/D_{22} = 2.50, 0.61, -1.45, -0.49$ for the components $ij = 11, 33, 13, 31$, respectively. The corresponding LES results are 2.90, 0.52, -1.10, -0.65. The agreement is not bad, but the model with isotropic timescale τ_{mod} underestimates the anisotropy of the diffusivity tensor.

Rubinstein & Barton (1991) show that the diffusivities depend strongly on the ratio P/ϵ for neutral flow. Using the measured value of P/ϵ they compute $D_{13}/D_{33} = 2.3$, which is close to the experimental result 2.2 (Tavoularis & Corrsin 1981) and in between the simulation results 2.5 (Rogers *et al.* 1989) and 2.1 (our data).

For increasing stratification, the anisotropy in terms of D_{22}/D_{33} increases strongly. As expected, vertical diffusion becomes much more suppressed than lateral diffusion

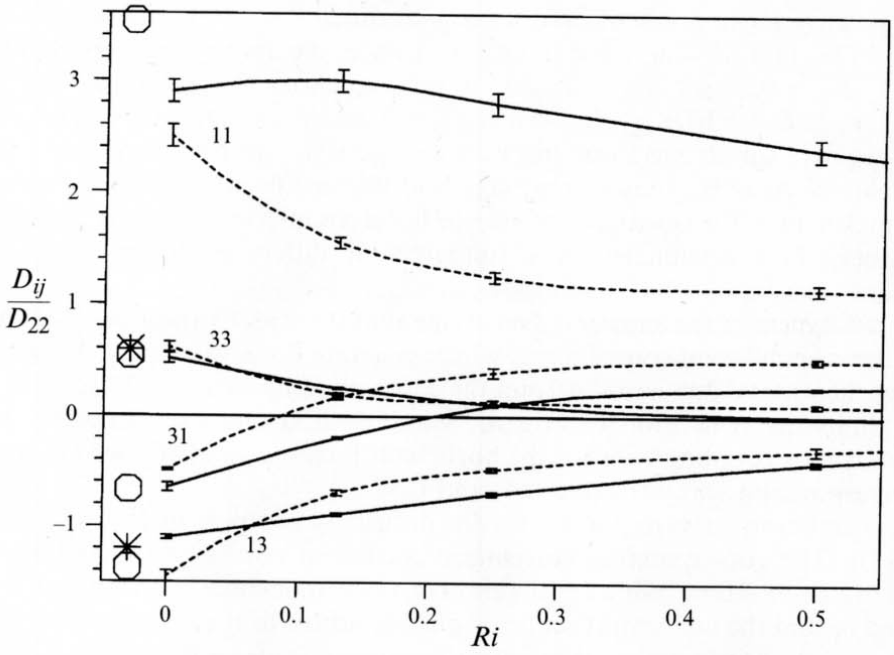

FIGURE 19. Components of the diffusivity tensor versus Richardson number. The full lines interpolate the mean values, the bars indicate the scatter; ○, results obtained by Rogers *et al.* (1989) for $Ri = 0$ (data taken from Rogers *et al.* 1986, run C128U); ✱, measurements by Tavoularis & Corrsin (1981, 1985) for $Ri = 0$, dashed line results from the SOC model, equation (17).

with increasing Ri. Conversely, buoyancy forces reduce the anisotropy in the horizontal plane in that D_{11}/D_{22} decreases slowly with Ri. D_{31} changes sign at $Ri \approx 0.2$ because buoyancy contributes more strongly than gradient fluxes to the production rate of $\overline{wc}_1$ for stable stratification. The SOC model also predicts this sign change. It might be remarkable that, in spite of vanishing vertical fluxes due to a vertical gradient (D_{33}), the positive vertical flux due to a downstream gradient (D_{31}) still persists.

Turbulent diffusion coefficients describe the mean transport properties of all scales. However, as was shown on the co-spectra of the vertical heat flux, the transport properties may vary over the wavenumber range. In spite of the almost vanishing coefficient D_{31} at $Ri = 0.13$, strong vertical fluxes of c_1 develop at large scales as well as at small scales but with opposite sign (figure 20*a*). The horizontal fluxes $\overline{uc}_1$ and $\overline{vc}_2$ are carried mainly by large scales (figure 20*b*). Therefore, we do not find significant differences of ratios D_{ij}/D_{22} of LES and DNS even at high Richardson numbers.

In view of the difficulties of modelling the diffusion tensor one may ask whether all components of D_{ij} are equally important for an accurate prediction of scalar dispersion in a turbulent shear flow. A rather simple analysis reveals that the tensor asymmetries are probably seldom relevant in practice, since the turbulent fluxes in the downstream direction are usually small in comparison to advective fluxes by the mean flow in that direction. Also, in real shear flows, downstream gradients are often small compared to vertical gradients. To illustrate this fact, we consider the transport equation which is satisfied by any concentration field in a homogeneous shear flow with constant diffusivities D_{ij}

$$\frac{\partial C}{\partial t} + U(z)\frac{\partial C}{\partial x} = D_{11}\frac{\partial^2 C}{\partial x^2} + D_{22}\frac{\partial^2 C}{\partial y^2} + D_{33}\frac{\partial^2 C}{\partial z^2} + (D_{13} + D_{31})\frac{\partial^2 C}{\partial x\,\partial z}. \tag{18}$$

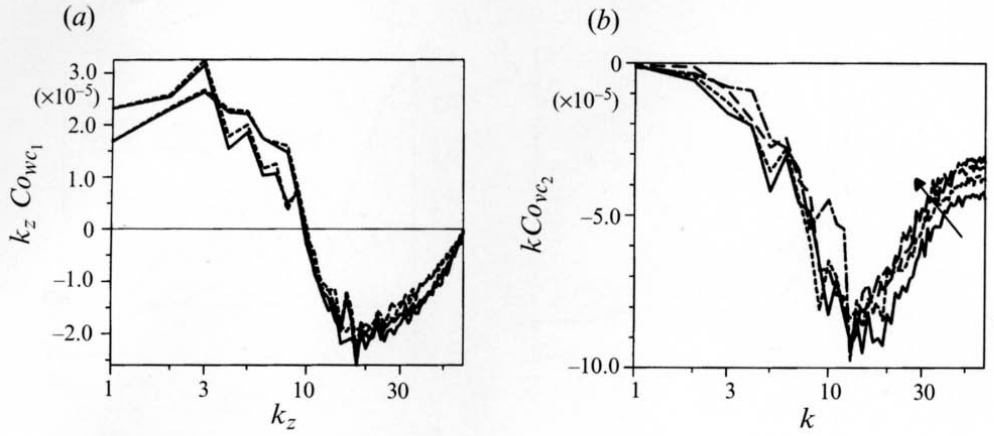

FIGURE 20. Co-spectra of scalar fluxes in variance preserving form. (*a*) Co-spectrum of flux $\overline{wc}_1$ versus vertical wavenumber k_z for $Ri = 0.13$ at $St = 8$ and 11; full lines $Pr_{SGS} = 1$, dotted lines $Pr_{SGS} = 0.5$. (*b*) Co-spectrum of cross-stream scalar flux $\overline{vc}_2$ versus spherical wavenumber k for $Ri = 0.25$ at $St = 5, 7, 9, 11$; arrow indicates increasing time.

In a concentration field C, which is initially constant in the vertical direction but driven by a uniform gradient in the downstream direction, a vertical concentration gradient $\partial C/\partial z = (\partial C/\partial x)\,St$ evolves under the action of shear. This vertical gradient is proportional to the shear time and, hence, may become much larger than the original downstream gradient. It follows from (18) that

$$\frac{\partial C}{\partial t} + U(z)\frac{\partial C}{\partial x} = (D_{11} + (D_{13} + D_{31})\,St + D_{33}(St)^2)\frac{\partial^2 C}{\partial x^2} + D_{22}\frac{\partial^2 C}{\partial y^2}. \tag{19}$$

From this equation we see that for large times, $St \gg 1$, the diffusivity tensor components D_{13} and D_{31}, and even more D_{11} become unimportant relative to D_{33} (and D_{22}). This also means that streamwise gradients are not likely to persist because they will quickly be smeared out by shear. Hence, the only tensor components of practical relevance are D_{33} and D_{22}.

4.3. *Diffusion of active and passive scalars with vertical gradients*

Up to now, we have determined the diffusion coefficients from the temperature field assuming that it evolves in the same manner as a passive scalar field c_3 with comparable vertical gradient. This was based on the fact that both fields evolve equally when starting from the same non-dimensional initial conditions. However, a passive scalar which is released statistically independently of θ may evolve differently because temperature has a significant influence on the dynamics whereas the scalar c_3 is simply advected by the motion field.

In order to quantify the possible differences, we performed simulations including an independent and passive scalar field c_3. The largest differences between a buoyant and a passive scalar are to be expected for strong stratification. We performed two simulations for $Ri = 0.5$. In the first case, a scalar concentration fluctuation c_3 was released at $St = 0$ with $c_3' = 0.05$ (using Gaussian random numbers); in the second case, c_3 was released at $St = 4$ with $c_3' = \theta'(St = 4) = 0.012$ (again using Gaussian random numbers). Both cases are treated using DNS and zero initial temperature fluctuations, as before. The first case resembles a flow where θ and c_3 pass through the same dynamical stages (same history) but differ in the initial r.m.s. value. In the second

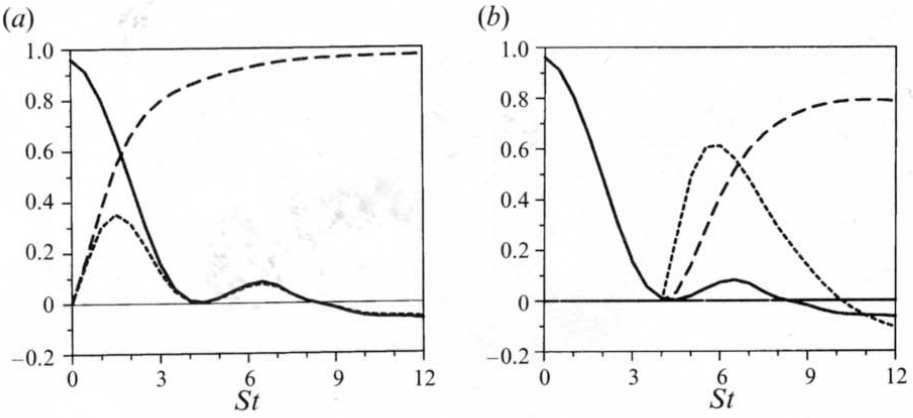

FIGURE 21. Correlation coefficients versus St (DNS data); (a) for release of c_3 at $St = 0$, (b) for release of c_3 at $St = 4$; ——, $-\overline{w\theta}/(w'\theta')$; ---, $-\overline{wc_3}/(w'c_3')$; ——, $\overline{\theta c_3}/(\theta' c_3')$.

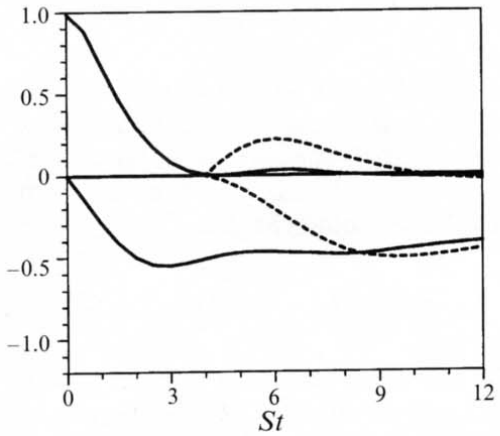

FIGURE 22. Normalized diffusivity tensor components D_{33}/D_{22} (upper curves) and D_{13}/D_{22} (lower curves) versus St computed by heat fluxes: ——, computed by scalar fluxes (release at $St = 4$): ----. The curves computed by the fluxes of the scalar released at $St = 0$ have been omitted since they are indistinguishable from the solid lines already for $St > 0.5$.

case, the passive scalar is released at a time when the magnitudes of the mean fluxes of momentum and heat pass through minimum values (see figure 4); hence it can be assumed that the differences in evolution of θ and c_3 will be largest for this case.

Figure 21 depicts results in terms of correlation coefficients of the vertical heat and scalar fluxes and of $\overline{\theta c_3}$. In both cases the coefficient $\overline{\theta c_3}/(\theta' c_3')$ reaches values of 0.8 or more, indicating that the passive scalar c_3 is captured by the same motion elements as the temperature. The resultant diffusivity ratios D_{33}/D_{22} and D_{13}/D_{22} (figure 22) are practically the same for both kinds of scalars. The largest differences occur with respect to the vertical fluxes in transient flow stages. In the case of early release, the correlation coefficients $\overline{wc_3}/w'c_3'$ and $\overline{w\theta}/w'\theta'$ become practically equal after $St = 3$. For late release, $\overline{wc_3}/w'c_3'$ undergoes a strong down-gradient and therefore mixing-dominated state before it finally approaches the small values achieved by $\overline{w\theta}/w'\theta'$ for $St > 11$.

The results indicate that the transport properties of a passive scalar with vertical gradient can be computed from those for temperature in the stratified medium.

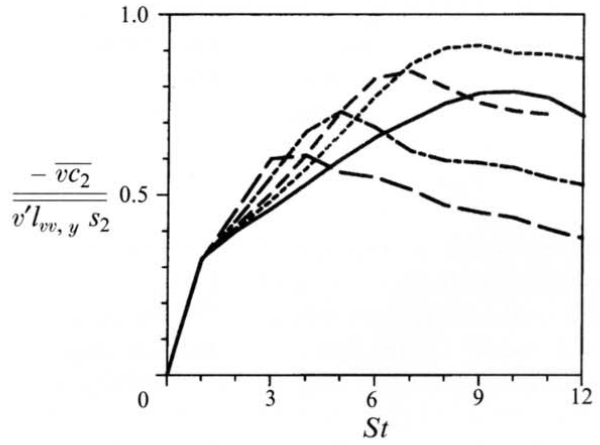

FIGURE 23. Test of mixing-length model, equation (20), for a flux driven by a cross-stream gradient. Line coding as in figure 2.

4.4. *Test of diffusivity models and other parameterizations*

In order to apply the above result, one needs simplified models to predict either D_{22} or D_{33} from the basic turbulence parameters. If one is known, the other can be determined from figure 19. A mixing-length approximation is

$$D_{11} = c_{11}\,u'l_{uu,x}, \quad D_{22} = c_{22}\,v'l_{vv,y}, \tag{20}$$

where c_{11} and c_{22} are open model coefficients. Values of the one-dimensional integral length scale $l_{uu,x}$ are given in table 1. Figure 23 shows the values of c_{22} computed from the simulations for various Ri. The coefficients become roughly stationary at late times. The coefficient c_{11} (not shown) varies between 1.2 ($Ri = 0$) and 0.4 ($Ri = 1$), c_{22} differs by 50% between the neutral and the strongly stratified case at $St = 12$. Both coefficients c_{11} and c_{22} are approximately equal for $St > 6$ for a given $Ri \geqslant 0.25$. Such simple mixing models are suitable for the horizontal fluxes because the horizontal fluxes are carried by rather large motion scales, as was shown in figure 20(*b*).

Various models have been proposed which express the vertical diffusivities $K_h \equiv D_{33}$ as $K_h = c_h \epsilon/N^2$ or $K_h = c_N w'^2/N$. The LES results for c_h and c_N are listed in table 2. For a further discussion see Schumann & Gerz (1994). Finally we test some parameterizations for the dissipation rate in stratified flows. The lengthscale ratio $l_\epsilon/(2l)$, where l_ϵ is defined by $\epsilon = q^3/l_\epsilon$, corresponds to the ratio of dissipative and turnover timescale τ_ϵ/τ. It decreases from 3.5 at $Ri = 0$ to 1.7 at $Ri = 1$ in the LES. This corroborates the proposal of Brost & Wyngaard (1978) that buoyancy should reduce the size of the dissipation lengthscale. However, we find that the computed ratio of l_ϵ and the buoyancy lengthscale $l_b = w'/N$ is much larger than unity. It grows steadily with time and reaches values in between 10 (for $Ri = 0.13$) and 40 (for $Ri = 1$) at $St = 12$. The dissipation of kinetic energy therefore does not scale with l_b, which agrees with the findings of Schumann (1991).

As an alternative, Hunt, Stretch & Britter (1988) proposed to choose the shear length $l_S = w'/S$ as the relevant lengthscale in order to parameterize the dissipation rate ϵ in shear flows. The coefficient A_S, defined by

$$\epsilon = A_S \frac{w'^3}{l_S} = A_S\, w'^2 S, \tag{21}$$

becomes stationary and depends only slightly on Ri during an early transient flow period. At late times A_S approaches values in between 0.54 and 0.62 (see table 2), which is surprisingly close to the estimate $A_S = 0.45$ that Hunt *et al.* (1988) deduced from the logarithmic law of the wall for neutral stationary boundary layers.

5. Conclusions

The dynamics and transport properties of homogeneous turbulence have been investigated for flows with uniform shear and with either neutral or stable uniform stratification. The LES method used extends the DNS method of Gerz *et al.* (1989) by a SGS model. The SGS model is very simple and may be improved in future studies. However, various arguments together with the parameter studies and comparisons between DNS and LES results indicate that the details of the SGS model are not very important, at least for $Ri \leqslant 0.25$. For $Ri \leqslant 0.5$, the computed normalized variances and covariances are within the range of data of a large set of measurements in laboratory and atmospheric flows. Also the growth rate, the shear number, and the shape of spectra agree generally well with experimental observations.

Of major concern for this study was the question whether the turbulent flow state becomes self-similar in the sense of approaching constant normalized flow statistics. For small to moderate Richardson numbers, such a self-similar state is reached after a shear time of about 6 when the initial value of the inverse Froude number $Fi = Nl/q$ is small. In strongly stratified situations, Ri no longer defines the flow state uniquely and the Froude number becomes an important additional parameter. For Fi greater than a critical value of about 3 turbulent mixing dies out. In this case the final statistics depend on the history of mixing in the past fully turbulent regime. In particular, flow history affects vertical fluxes of both heat and momentum at low wavenumbers (large scales). Hence, we expect that the results for strong stratification depend on details of the initial conditions, and this should be studied in the future.

We find that the LES and DNS give very similar results for weak stratification when the constant molecular viscosity of the DNS is set equal to the mean turbulent viscosity of the LES. For a given resolution, the LES resolves a wider range of energetic scales and thus gives a better approximation to high-Reynolds-number turbulence than a DNS. Also, the more energetic motions in the medium wavenumber range cause the inverse Froude number to grow less quickly so that mixing persists longer. Hence the LES results depend less on flow history than the DNS results. Finally, the LES adjusts its SGS diffusivities to the growing or decreasing level of small-scale turbulence energy. This makes the LES method superior to the DNS for studies of high-Reynolds-number flows and allows for a wider range of Richardson and Froude numbers. The self-adjusting property of the LES becomes particularly important in the case of shear flow at strong stratification because then decay rates are significantly higher than in shear-free stratified cases (Gerz & Schumann 1991).

Comparisons between results from simulations with 96^3 and 128^3 grid points suggest that the results are only weakly sensitive to the SGS model and the numerical approximations with respect to large-scale flow properties. However, such grids are much too coarse to resolve the inertial subrange of turbulence. Therefore, the results for small-scale properties depend on the details of the SGS model. In particular, the computed rate of dissipation depends on c_{SGS}, and the scalar dissipation at large inverse Froude numbers depends also on the SGS Prandtl number. The grid sensitivity study also reveals that the flow evolution is not yet independent on the value of the effective Reynolds number.

For neutral stratification, the turbulence energy grows about exponentially with time approaching a constant shear number and a constant growth rate of approximately $F = 1.5$. The state of turbulence changes very slowly near a stationary Richardson number for which our simulations indicate a value of about 0.13. The values of the computed growth rate and the stationary Richardson number depend on details of the SGS model similarly but less strongly as DNS results depend on the Reynolds number.

For the first time, the diffusivity tensor has been computed for stably stratified turbulence using the LES approach. The results corroborate our previous DNS analysis (Kaltenbach *et al.* 1991). The diffusivity tensor is strongly anisotropic with $D_{11} > D_{22} > D_{33}$ and asymmetric, i.e. $D_{13} \neq D_{31}$. However, for practical applications, the only essential diffusivity parameters are D_{22} and D_{33} because streamwise gradients are not likely to persist in a shear flow. The ratio D_{33}/D_{22} decreases from about 0.6 for neutral flows down to values below 0.01 for $Ri > 0.5$. For small Richardson numbers, buoyant and passive scalars with vertical mean gradients behave similarly. Some decorrelation between such scalars does occur for strong stratification at times when the fluxes are already small compared to those in the initial period. To a good approximation, the transport properties of a passive scalar with vertical gradient can be computed from those for temperature in the stratified medium.

A severe limitation of the present simulations arises from the fact that vertical turbulent diffusivities $D_{33} = K_h$ and K_m become smaller than the molecular or SGS diffusivity when the Richardson number exceeds 0.5 in the LES (0.25 in the DNS). Turbulent horizontal diffusivities, however, remain considerably larger than their molecular/SGS-counterparts and are therefore more reliable than the results concerning vertical turbulent diffusion. For strongly stratified situations and large inverse Froude numbers the vertical fluxes may become counter-gradient at small and at large wavenumbers. The details of these fluxes at small wavenumbers depend upon the flow history and those at large wavenumbers on the Prandtl number. However, the magnitude of these fluxes is so small that they are hardly of practical relevance in most applications.

The data set from LES has been used in order to test simple models. Downstream and cross-stream transports, which are always down-gradient and mainly carried by the most energetic motion scales, can be described by a mixing-length approximation. SOC models give about the right trends for the components of the diffusivity tensor but cannot describe the strong anisotropy. The task remains to deduce more accurate models which account for the anisotropy of the turbulence structure and for the reduction of mixing at large inverse Froude numbers. The relation $\epsilon = A_S w'^2 S$ as proposed by Hunt *et al.* (1988) provides a good estimate for the dissipation rate in neutral as well as in stratified shear flows with $Ri < 1$.

This study was supported by the Volkswagenstiftung under the auspices of the DECHEMA. Part of this work was also supported by the Deutsche Forschungsgemeinschaft. We thank Dr A. Dörnbrack for providing the results of his SOC model analysis. Several comments by the reviewers motivated us to examine the role of the SGS-model in greater detail and to include additional DNS results.

Appendix: Transport equations

From the equations of motions follow 'transport equations' for the non-vanishing variances and covariances of homogeneous turbulent fluctuations,

$$\partial\overline{uu}/\partial t = -2\overline{uw}S + \phi_{11} - \epsilon_{11}, \tag{22}$$

$$\partial\overline{vv}/\partial t = \phi_{22} - \epsilon_{22}, \tag{23}$$

$$\partial\overline{ww}/\partial t = 2\beta g\overline{w\theta} + \phi_{33} - \epsilon_{33}, \tag{24}$$

$$\partial\overline{uw}/\partial t = -\overline{ww}S + \beta g\overline{u\theta} + \phi_{13} - \epsilon_{13}, \tag{25}$$

$$\partial\overline{u\theta}/\partial t = -\overline{uw}s - \overline{w\theta}S + \phi_{1\theta} - \epsilon_{1\theta}, \tag{26}$$

$$\partial\overline{w\theta}/\partial t = -\overline{ww}s + \beta g\overline{\theta\theta} + \phi_{3\theta} - \epsilon_{3\theta}, \tag{27}$$

$$\partial\overline{\theta\theta}/\partial t = -2\overline{w\theta}s - \epsilon_{\theta}. \tag{28}$$

A related balance exists for the available potential energy $E_{pot} = \frac{1}{2}\beta g\overline{\theta^2}/s = \frac{1}{2}N^2\overline{\theta^2}/s^2$. The kinetic energy $E_{kin} = \frac{1}{2}q^2$ satisfies

$$\tfrac{1}{2}\partial q^2/\partial t = -\overline{uw}S + \beta g\overline{w\theta} - \epsilon = P - B - \epsilon = (F-1)\,\epsilon, \tag{29}$$

and the budget of the total energy $E_{tot} = E_{kin} + E_{pot}$ is independent of the vertical heat flux which converts kinetic energy into potential energy and vice versa,

$$\partial E_{tot}/\partial t = -\overline{uw}S - \epsilon - \chi. \tag{30}$$

Here, the pressure-interaction terms are denoted by

$$\phi_{ij} = \frac{1}{\rho}\overline{p(\partial u_i/\partial x_j + \partial u_j/\partial x_i)}, \quad \phi_{i\theta} = \frac{1}{\rho}\overline{p(\partial\theta/\partial x_i)}. \tag{31}$$

In the LES, the dissipation terms result from the subgrid fluxes, $\tau_{ij} = \overline{u_i' u_j'}$ and $\tau_{i\theta} = \overline{u_i'\theta'}$ as

$$\epsilon_{ij} = \overline{\left(u_j\frac{\partial\tau_{ik}}{\partial x_k} + u_i\frac{\partial\tau_{jk}}{\partial x_k}\right)}, \quad \epsilon_{i\theta} = \overline{\left(u_i\frac{\partial\tau_{\theta k}}{\partial x_k} + \theta\frac{\partial\tau_{ik}}{\partial x_k}\right)}, \quad \epsilon_{\theta} = 2\overline{\left(\theta\frac{\partial\tau_{\theta k}}{\partial x_k}\right)},$$

$\epsilon = \frac{1}{2}\epsilon_{ii}$, and $\chi = \beta g\epsilon_{\theta}/(2s)$. The subgrid fluxes are parametrized as $\tau_{ij} = -2\nu_t S_{ij}$ and $\tau_{i\theta} = -(\nu_t/Pr_{SGS})(\partial\theta/\partial x_i)$, using (1).

REFERENCES

Brost, R. A. & Wyngaard, J. C. 1978 A model study of the stably-stratified planetary boundary layer. *J. Atmos. Sci.* **35**, 1427–1440.

Corrsin, S. 1974 Limitations of gradient transport models in random walks and in turbulence. *Adv. Geophys.* **18A**, 25–60.

Dörnbrack, A. 1991 Tensor der turbulenten Diffusion – Eigenschaften und Anwendungen. *Met. Rdsch.* **44**, 73–79.

Ellison, T. H. 1957 Turbulent transport of heat and momentum from an infinite rough plane. *J. Fluid Mech.* **2**, 456–466.

Freeman, B. E. 1977 Tensor diffusivity of a trace constituent in a stratified boundary layer. *J. Atmos. Sci.* **34**, 124–136.

Galperin, B. 1986 A modified turbulent energy model for diffusion from elevated and ground point sources in neutral boundary layers. *Boundary-Layer Met.* **37**, 245–262.

Germano, M., Piomelli, U., Moin, P. & Cabot, W. 1991 A dynamic subgrid-scale eddy viscosity model. *Phys. Fluids* A **3**, 1760–1765.

Gerz, T. 1991 Coherent structures in stratified turbulent shear flows deduced from direct simulations. In *Turbulence and Coherent Structures* (ed. O. Métais & M. Lesieur), pp. 449–468. Kluwer.

Gerz, T. 1993 Vortex structure and persistent counter-gradient fluxes. In *Dynamics and Geometry of Vortical Structures, EUROMECH 305, Cortona, 28–30 June 1993*, pp. 13–14.

Gerz, T. & Schumann, U. 1989 Influence of initial conditions on the development of stratified homogeneous turbulent shear flow. In *Finite Approximations in Fluid Mechanics II, Notes on Numerical Fluid Dynamics* (ed. E. H. Hirschel), vol. 25, pp. 142–156. Vieweg.

GERZ, T. & SCHUMANN, U. 1991 Direct simulation of homogeneous turbulence and gravity waves in sheared and unsheared stratified flows. In *Turbulent Shear Flow 7* (ed. F. Durst, B. E. Launder, W. C. Reynolds, F. W. Schmidt & J. H. Whitelaw), pp. 27–45. Springer.

GERZ, T., SCHUMANN, U. & ELGHOBASHI, S. E. 1989 Direct numerical simulation of stratified homogeneous turbulent shear flows. *J. Fluid Mech.* **200**, 563–594.

HOLLOWAY, G. 1988 The buoyancy flux from internal gravity wave breaking. *Dyn. Atmos. Oceans* **12**, 107–125.

HOLT, S. E. 1990 The evolution and structure of homogeneous stably stratified sheared turbulence. PhD dissertation, Dept of Civil Engng, Stanford University, Stanford CA.

HOLT, S. E., KOSEFF, J. R. & FERZIGER, J. H. 1992 A numerical study of the evolution and structure of homogeneous stably stratified sheared turbulence. *J. Fluid Mech.* **237**, 499–539.

HOPFINGER, E. J. 1987 Turbulence in stratified fluids: A review. *J. Geophys. Res.* **92**, 5287–5303.

HUNT, J. C. R. & CARRUTHERS, D. J. 1990 Rapid distortion theory and the 'problems' of turbulence. *J. Fluid Mech.* **212**, 497–532.

HUNT, J. C. R., KAIMAL, J. C. & GAYNOR, J. E. 1985 Some observations of turbulence structure in stable layers. *Q. J. R. Met. Soc.* **111**, 793–815.

HUNT, J. C. R., STRETCH, D. D. & BRITTER, R. E. 1988 Length scales in stably stratified turbulent flows and their use in turbulence models. In *Stably Stratified Flows and Dense Gas Dispersion* (ed. J. S. Puttock), pp. 285–321. Clarendon.

ITSWEIRE, E. C., HELLAND, K. N. & VAN ATTA, C. W. 1986 The evolution of grid-generated turbulence in a stably stratified fluid. *J. Fluid Mech.* **162**, 299–338.

ITSWEIRE, E. C., KOSEFF, J. R., BRIGGS, D. A. & FERZIGER, J. H. 1993 Turbulence in stratified shear flows: implications for interpreting shear-induced mixing in the ocean. *J. Phys. Ocean.* **23**, 1508–1522.

IVEY, G. N. & IMBERGER, J. 1991 On the nature of turbulence in a stratified fluid. Part I: The energetics of mixing. *J. Phys. Ocean.* **21**, 650–658.

KALTENBACH, H.-J. 1992 Turbulente Diffusion in einer homogenen Scherströmung mit stabiler Dichteschichtung. Diss. TU München, report DLR-FB 92-26, 142 pp.

KALTENBACH, H.-J., GERZ, T. & SCHUMANN, U. 1991 Transport of passive scalars in neutrally and stably stratified homogeneous turbulent shear flows. In *Advances in Turbulence 3* (eds. A. Johansson & H. Alfredsson), pp. 327–334. Springer.

KOMORI, S., UEDA, H., OGINO, F. & MIZUSHINA, T. 1983 Turbulence structure in stably stratified open-channel flow. *J. Fluid Mech.* **130**, 13–26.

LAUNDER, B. E. 1978 Heat and mass transport. In *Turbulence* (ed. P. Bradshaw), pp. 231–287. Springer.

LIENHARD, J. H. & VAN ATTA, C. W. 1990 The decay of turbulence in thermally stratified flow. *J. Fluid Mech.* **210**, 57–112.

LILLY, D. K. 1967 The representation of small-scale turbulence in numerical simulation experiments. Proc. IBM Sci. Comput. Symp. on Environmental Sci., Nov. 14–16, 1966, Thomas J. Watson Res. Center, Yorktown Heights, NY, IBM Form no. 320–1951, pp. 195–210.

LILLY, D. K., WACO, D. E. & ADELFANG, S. I. 1974 Stratospheric mixing estimated from high-altitude turbulence measurements. *J. Appl. Met.* **13**, 488–493.

MASON, P. J. & DERBYSHIRE, H. 1990 Large-eddy simulations of the stably-stratified atmospheric boundary layer. *Boundary-Layer Met.* **53**, 117–162.

MÉTAIS, O. & HERRING, J. R. 1989 Numerical simulation of freely evolving turbulence in stably stratified fluids. *J. Fluid Mech.* **202**, 117–148.

MÉTAIS, O. & LESIEUR, M. 1992 Spectral large-eddy simulation of isotropic and stably stratified turbulence. *J. Fluid Mech.* **239**, 157–194.

MOIN, P., SQUIRES, K., CABOT, W. & LEE, S. 1991 A dynamic subgrid-scale model for compressible turbulence and scalar transport. *Phys. Fluids* A **3**, 2746–2757.

MONIN, A. S. & OZMIDOV, R. V. 1985 *Turbulence in the Ocean.* Dordrecht: Reidel. 247 pp.

MOREL, R., ALCARAZ, E., AYRAULT, M., ZEGADI, R. & MEJEAN, P. 1991 Effects of thermal stable stratification on turbulent boundary layer characteristics. *Atmos. Environ.* **25A**, 1263–1269.

NIEUWSTADT, F. T. M. 1984 The turbulent structure of the stable, nocturnal boundary layer. *J. Atmos. Sci.* **41**, 2202–2216.

RICHARDSON, L. F. 1920 The supply of energy from and to the atmospheric eddies. *Proc. R. Soc. Lond.* A **97**, 354–373.

ROGALLO, R. S. & MOIN, P. 1984 Numerical simulation of turbulent flows. *Ann. Rev. Fluid Mech.* **16**, 99–137.

ROGERS, M. M., MANSOUR, N. N. & REYNOLDS, W. C. 1989 An algebraic model for the turbulent flux of a passive scalar. *J. Fluid Mech.* **203**, 77–101.

ROGERS, M. M., MOIN, P. & REYNOLDS, W. C. 1986 The structure and modeling of the hydrodynamic and passive scalar fields in homogeneous turbulent shear flow. *NASA Rep.* TF-25, Dept Mech. Engng, Stanford University.

ROHR, J. J. 1985 An experimental study of evolving turbulence in uniform mean shear flows with and without stable stratification. PhD dissertation, University of California, San Diego.

ROHR, J. J., ITSWEIRE, E. C., HELLAND, K. N. & VAN ATTA, C. W. 1988*a* An investigation of the growth of turbulence in a uniform-mean-shear flow. *J. Fluid Mech.* **187**, 1–33.

ROHR, J. J., ITSWEIRE, E. C., HELLAND, K. N. & VAN ATTA, C. W. 1988*b* Growth and decay of turbulence in a stably stratified shear flow. *J. Fluid Mech.* **195**, 77–111.

RUBINSTEIN, R. & BARTON, J. M. 1991 Renormalization group analysis of anisotropic diffusion in turbulent shear flows. *Phys. Fluids* A **3**, 415–421.

SCHMIDT, H. & SCHUMANN, U. 1989 Coherent structure of the convective boundary layer derived from large eddy simulations. *J. Fluid Mech.* **200**, 511–562.

SCHUMANN, U. 1975 Subgrid scale model for finite difference simulations of turbulent flows in plane channels and annuli. *J. Comput. Phys.* **18**, 376–404.

SCHUMANN, U. 1987 The counter-gradient heat-flux in turbulent stratified flows. *Nucl. Engng Des.* **100**, 255–262.

SCHUMANN, U. 1991 Subgrid length-scales for large-eddy simulation of stratified turbulence. *Theoret. Comput. Fluid Dyn.* **2**, 279–290.

SCHUMANN, U. & GERZ, T. 1994 Turbulent mixing in stably stratified homogeneous turbulence. *J. Appl. Met.* (in press).

SHIRANI, E., FERZIGER, J. H. & REYNOLDS, W. C. 1981 Mixing of a passive scalar in isotropic and sheared homogeneous turbulence. *Rep. no.* TF-15, Thermosciences Division, Dept of Mech. Engng, Stanford University, Stanford, CA.

STILLINGER, D. C., HELLAND, K. H. & VAN ATTA, C. W. 1983 Experiments on the transition of homogeneous turbulence to internal waves in a stratified fluid. *J. Fluid Mech.* **131**, 91–122.

TAVOULARIS, S. & CORRSIN, S. 1981 Experiments in nearly homogeneous turbulent shear flow with a uniform mean temperature gradient, Part 1. *J. Fluid Mech.* **104**, 311–347.

TAVOULARIS, S. & CORRSIN, S. 1985 Effects of shear on the turbulent diffusivity tensor. *Intl. J. Heat Mass Transfer* **28**, 265–276.

TAVOULARIS, S. & KARNIK, U. 1989 Further experiments on the evolution of turbulent stresses and scales in uniformly sheared turbulence. *J. Fluid Mech.* **204**, 457–478.

TSARENKO, V. M. 1989 Determination of the turbulent diffusion tensor in a stratified atmospheric surface layer. *Izv. Atmos. Oceanic Phys.* **25**, 189–194.

TSARENKO, V. M. & YAGLOM, A. M. 1991 Semiempirical theories for turbulent diffusion in a neutrally stratified atmospheric surface layer. *Phys. Fluids* A **3**, 2199–2206.

WEBSTER, C. A. G. 1964 An experimental study of turbulence in a density-stratified shear flow. *J. Fluid Mech.* **19**, 221–245.

YAMADA, T. 1977 A numerical experiment on pollutant dispersion in a horizontally-homogeneous atmospheric boundary layer. *Atmos. Environ.* **11**, 1015–1024.

YOON, K. & WARHAFT, Z. 1990 The evolution of grid generated turbulence under conditions of stable thermal stratification. *J. Fluid Mech.* **215**, 601–638.